Novel Multiband and Broadband Metamaterial Absorber for RCS reduction and EM shielding.

By

Muhammad Saad Mahfooz

MS (EE)-27
00000397959

Supervisor

Dr. Abdul Wakeel

Co-Supervisor

Dr. Adil Masood Siddiqui

The thesis submitted in partial fulfillment of the requirements for the degree

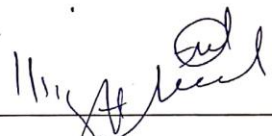of Masters of Science in Electrical Engineering (MSEE)

at

Military College of Signals (MCS),
National University of Sciences and Technology (NUST),
Islamabad, Pakistan.

(June 2023)

THESIS ACCEPTANCE CERTIFICATE

Certified that final copy of MS/MPhil thesis written by Mr. **P-8810 PN M Saad Mahfooz,** Registration No. **00000397959** of **Military College of Signals** has been vetted by undersigned, found complete in all respect as per NUST Statutes/Regulations, is free of plagiarism, errors and mistakes and is accepted as partial, fulfillment for award of MS/MPhil degree. It is further certified that necessary amendments as pointed out by GEC members of the student have been also incorporated in the said thesis.

Signature: _____

Name of Supervisor **Asst Prof Abdul Wakeel, PhD**

Date: _____

Signature (HoD): _____

Brig
HoD
Dept of Elec Engg
Military College of Signals (NUST)
(NUST Campus)

Date: _____

Signature (Dean): _____

Date: 25/7/23

Brig
Dean, MCS (NUST)
(Asif Masood, Phd)

ii

I express my heartfelt gratitude to my parents, spouse, and esteemed faculty members for their unwavering and invaluable support throughout my academic journey, and it is with immense gratitude that I dedicate this work to them.

Certificate of Originality

It is certified that the work produced by me in this thesis is solely based on my research to the best of my knowledge and understanding of metamaterials. It neither consists of any previously published material nor results produced are copied or taken as in any form from the literature of the subject field. It is neither any extension of the previously accepted or published literature anywhere or in NUST MCS to the best of my understanding and knowledge. Any collaborations and contributions done by any of my colleagues and superiors are mentioned in my thesis in true letter and spirits. I have not taken any design or material from any author and collaborator currently working or have worked in the subject field of metamaterials.

It is also declared that the material, results, ideas, and experimental verifications done by me during research are true in any form and are not in any form manipulated or fake in any form. I have designed the metasurfaces and performed its analysis, design simulations, results and publications based on my understanding and expertise with exceptional help from my supervisor and his guidance. The work done in this thesis belongs solely to me and the ownership of my work belongs to NUST MCS. Any material in this research thesis may not be made available to any third party without prior permission from MCS authorities.

Author Name: <u>M Saad Mahfooz</u>

Reg# 00000397959

Signature: _____

Acknowledgement

Abstract

Metasurfaces are artificial structures carefully designed to exhibit extraordinary characteristics, including the ability to exhibit negative refractive index, negative permittivity, and negative permeability as well, which are unattainable in naturally occurring materials. These subwavelength designs have found extensive applications and offer enhanced efficiency in various fields, including solar energy harvesting, electromagnetic (EM) shielding, beam splitting, and more. Although classical techniques like the Faraday effect and bi-refringence can achieve perfect absorption of EM waves, they often come with drawbacks such as increased costs, design complexity, structural non-linearities, and bulkiness. Consequently, metasurface-based perfect absorbers have earned significant interest among researchers over the past two decades and continue to be actively explored. Perfect absorption can be achieved through the design of left-handed metamaterials (LHMs), which reduce losses and provide negative permittivity and permeability. Numerous LHMs have been proposed in the literature; however, many designs lack angular stability and polarization insensitivity.

In this thesis, we present three metasurface designs. The first design is a tetra-band metasurface absorber intended for X and Ku band applications. It is based on the concept of Split Ring Resonators (SRRs) and utilizes an FR-4 substrate. The proposed design exhibits four distinct absorption peaks, with polarization insensitivity up to 90˚ and an angular stability of 60˚. Subsequently the 2ⁿᵈ design entails a wideband metamaterial absorber (MA) that proves to be highly suitable for deployment across a diverse range of energy bands, specifically encompassing the C, X, K, and Ku frequencies. The structured MA design incorporates Cyclic-4 (C-4) symmetry, having excellent angular stability and showing excellent response to polarization insensitivity till 90˚, which a huge achievement in case of broad band meta surfaces. The design features a modified square ring-shaped structure implemented on a FR-4 economical substrate, utilizing SMT resistors to achieve a high absorptivity of 99%.

The third design is a frequency-tunable metasurface employing resistors, inductors, and diodes. This design enables the metasurface to switch bands from X-band to Ku-band by toggling the diodes on and off. Various parametric analyses and modifications were conducted to optimize absorption. An in-depth analysis of surface current and electric field

distributions was conducted with the aim of comprehending the intricate absorption mechanisms at play. To evaluate the simulated results the above designs MAs were fabricated, and it has been observed that the simulated and experimental results have shown good agreement with each.

The designed meta surfaces have extensive applications related to radar stealth material, energy harvesting, and various microwave applications. It is worth noting that our planar, symmetric, single-layered, and passive-elements-based MA design achieves superior accuracy compared to previous studies.

Contents Table

Chapter 4..**42**

Ultra-thin, Wideband Modified Square Shaped with Chip resistors Metamaterial Absorber for RCS reduction applications.

Chapter 5..**60**

Design methodology and Simulation Analysis of the Designed Reconfigurable MA

List of Figures

List of Acronyms

LTC   Linear to circular

CST   Computer simulation tool

PCR   Polarization conversion ratio

ε Permittivity

μ Permeability

CPC   Cross polarization conversion

RCS   Radar Cross-Section

FRC   Frequency Reconfigurable

QWP   Quarter-wave plate

HWP   Half-wave plate

CHAPTER 1

Introduction

The chapter consists of theoretical background and motivation related to the below mentioned thesis. The importance of meta surface has also been highlighted along with the objectives outlined in the last section.

1.1   Understanding Polarization

The polarization of electromagnetic (EM) waves holds great significance within the scientific community. EM waves exhibit three primary polarization types: linear, circular, and elliptical. Linear polarization occurs when the electric field lies in a single plane, either horizontally or vertically. Circularly polarized EM waves involve one of the vector components, either x or y, being out of phase by 90° with respect to the other. Additionally, the above-mentioned types can be seen as special cases of elliptical polarization. Each of these polarization types offers unique advantages over the others.

Extensive research has been conducted to manipulate the polarization of EM waves. Various techniques have been developed to convert one polarization form into another or to achieve perfect absorption. EM wave absorption carries numerous benefits and has thus become a subject of significant research within the field. Absorbers have gained substantial attention due to their potential for industrial-level applications. Initially, the focus was primarily on achieving metamaterial absorbers through the Faraday effect. However, these 3D metamaterial designs proved to be costly, complex, and prone to system non-linearities. Recent advancements have provided simpler methods and techniques for designing 2D metasurfaces as alternatives to 3D metamaterial absorbers. These metasurfaces are easier to design and fabricate, offering greater flexibility and lower costs. The subsequent section will delve into the detailed importance of metasurfaces.

1.2   The Metasurfaces

Metamaterials are artificially structured designs that possess unique properties that are not present in nature [1]. Based on their geometry, metamaterials can be categorized as either 2D or 3D structures. Unlike traditional metamaterials, 2D metasurfaces are ultrathin and consist of a periodic array with repeating unit cells alongside the x and y axes. It is crucial for the thickness of the substrate to be below the wavelength scale [2-4]. The material properties, including conductivity, permittivity, and loss tangent, used in the design and fabrication of these structures, hold significant importance as they actively contribute to the behavior and performance of the overall design. The design principles governing the geometrical configuration of the unit cell of MA play a central role and will be discussed in subsequent chapters. Fig. 1.1 illustrates a metasurface composed of single split-ring resonators (SRRs) unit cells repeated along the x and y directions [5]. These 2D periodic metasurfaces can operate in two modes: reflection and transmission. Figure 1.2 showcases a metasurface with a cyclic-4 symmetrical unit cell design, enabling it to function as a perfect absorber [6].

Each mode of operation, whether reflection or absorption, carries its own significance and application viewpoint. Metasurfaces designed for reflection and absorption modes incorporate a ground plane, which restricts wave transmission and induces total internal reflection. On the other hand, metasurfaces operating in transmission mode do not require a ground plane. In the subsequent sections, a comprehensive analysis will be conducted to classify metasurfaces, providing relevant examples to support the discussion.
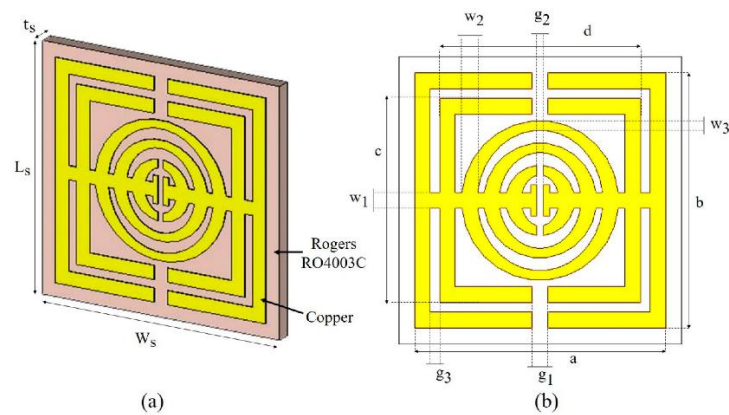
Figure 1.1: Metasurface consists of repeating split-ring resonator [5]
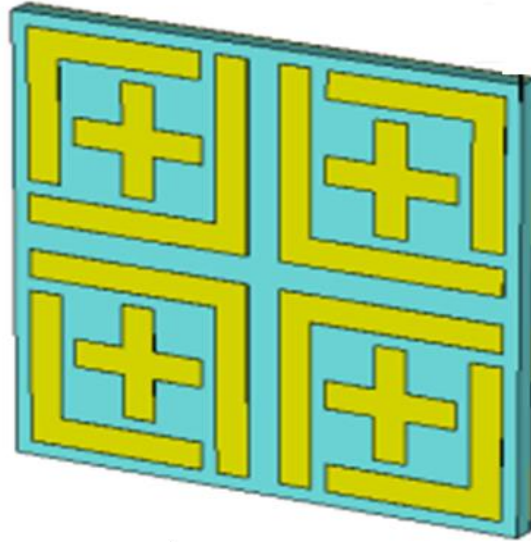
Figure 1.2: Metasurface absorber consists of repeating split-ring resonator [6]

Different techniques for the modes of operations have been realized in literature while considering meta surfaces. Most significant techniques are discussed below with examples.

1.2.1   Anisotropic Metasurfaces

The geometrical configuration of the unit cell plays a crucial role in metasurfaces' ability to convert polarization, primarily due to anisotropy. Anisotropy refers to the non-identical configuration of a unit cell when it is split along different axes. Figure 1.3, illustrating a double triangle unit cell design, can help illustrate this concept [7]. If the unit cell is split in half along the x-axis, the geometry of each half after splitting should not be the same as when it is split along the y-axis. This anisotropic behavior is exemplified in the structure depicted in Fig. 1.3, which represents reflection mode in which an anisotropic metasurface operates. When the unit cell is split along the x and y axes, the geometrical configuration should differ for each half. Anisotropy is a desirable characteristic in metasurfaces as it leads to a distribution of current within the structure which is non-uniform. In summary, the anisotropy resulting from the unit cell's geometry is a fundamental aspect of polarization conversion in metasurfaces. It is responsible for creating non-uniform current distributions, contributing to the meta surface's ability to manipulate polarization.
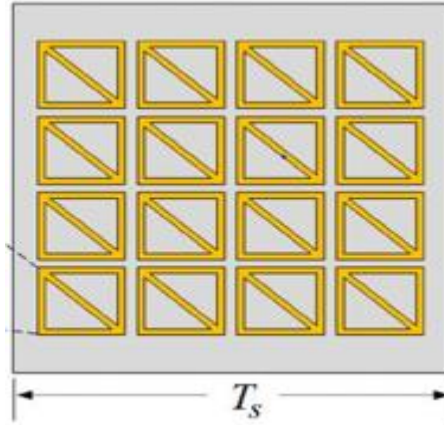
Figure 1.3: (a) Anisotropic unit cell design of metasurface [7]

1.2.2 Chiral Metasurfaces

Polarization conversion is effectively demonstrated using chiral metasurfaces, which leverage the generation of electromagnetic coupling at distinct resonant frequencies [8,9]. Chirality refers to the absence of mirror symmetry in the structure, as illustrated in Fig.1.4. Within this arrangement, patches are strategically situated on both the upper and lower surfaces of the substrate. Notably, these patches are rotated relative to each other. Consequently, chiral metasurfaces exhibit asymmetrical transmission patterns. This can be observed through the distinct responses of the transmission coefficients in both forward and backward directions. Researchers widely employ this technique to achieve polarization conversion and realize asymmetrical transmission.
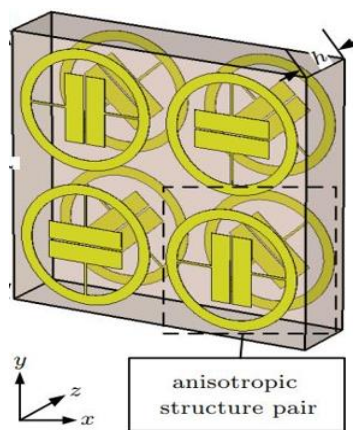
Figure 1.4: Chiral structure of discussed metasurface [8]

1.2.3   Metasurface Absorbers

Metasurface absorbers are specifically designed to selectively absorb a desired frequency band or peak. These absorbers are characterized by a four-fold or cyclic-4 (C4) symmetrical structural design, wherein the structure maintains the same pattern after every 90˚ rotation [10]. Upon splitting the unit cell along the x-axis, the resulting geometric configuration of each half should mirror the identical pattern obtained when splitting it along the y-axis. This adherence to cyclic-4 symmetrical design principles can be observed in the structure illustrated in Fig.1.5, depicting a C4 symmetrical metasurface operating in absorption mode. Suppose the unit cell of this structure is split in two halves along the x-axis and y-axis, it should exhibit the same geometrical configuration for both halves. The C4 symmetry is highly desirable in metasurfaces as it enables efficient absorption of electromagnetic waves within   structure.
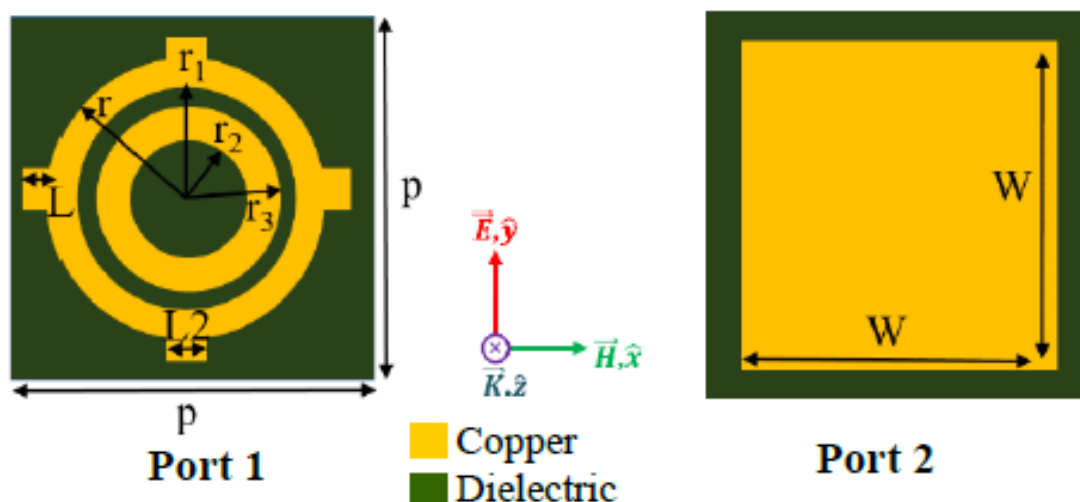
Figure 1.5: Absorber structure of discussed metasurface [10]

1.2.4   Applications of Metasurfaces

Metasurfaces offer numerous advantages, including a compact profile, seamless integration on chips, and straightforward fabrication processes. As a result, they find applications in various fields, such as enhancing antenna radiation, suppressing scattering, reducing radar cross-section, and enhancing gains through focusing lenses [11-13]. Additionally, metasurfaces play a crucial role in polarization beam splitting and beam deflection. Researchers have successfully demonstrated the independent manipulation of circular and linear polarized waves using metasurfaces [14].

6

Plasmonic metasurfaces have significant potential in optical communications, offering opportunities for high-capacity communication, real-time holography, and adaptive optics [15]. In the context of this thesis, we introduce a unique metasurface absorber that encompasses a broad spectrum of applications across different frequency bands which includes C, X, Ku, K, and Ka.

1.3   Objectives and Motivation

In the past decade, there has been a remarkable surge in the development of metasurface absorbers for efficient absorption of electromagnetic (EM) waves. These planar, ultra-thin metasurface absorbers offer significant advantages compared to previously employed techniques such as the Faraday effect, Brewster effect, and optical cavity of crystals. These conventional techniques were used for operations like polarization conversion, beam-splitting, and absorption. However, the advent of metasurface absorbers has opened up new possibilities due to their unique characteristics. Researchers are actively engaged in the pursuit of ultra-thin, multi-functional, broadband, efficient, and angular stable metasurface absorbers for various real-world applications. The aim is to develop metasurfaces that can absorb EM waves effectively across a wide range of frequencies, while also maintaining stability under different incident angles. Working principle of meta material absorbers is defined by [16]:

$$A(\omega) = 1 - |S11(\omega)| - |S21(\omega)| \qquad (1.1)$$

In the context of the given scenario, |S11(ω)| and |S21(ω)| represent the magnitudes of the reflectivity and transmissivity coefficients, respectively. It is apt to mention that the presence of a ground plane results in complete reflection, leading to the absence of any transmission. Consequently, |S21(ω)| is equal to zero. The Equation (1.1) can then be written as

$$A(\omega) = 1 - S11(\omega) \qquad (1.2)$$

Moreover, for normally incident electromagnetic wave, $|S11(\omega)|$ can be written as

$$|S11(\omega)| = \frac{(Z(\omega) - Zo)}{(Z(\omega) + Zo)} \qquad (1.3)$$

In the given context, Z(ω) represents the impedance of the metamaterial absorber (MA),

while Zo = 377 Ω is known as free space impedance. The absorption phenomenon manifests itself when the impedance Z(ω) approaches a critical threshold, Zo, resulting in the magnitude of the reflection coefficient, |S11(ω)|, converging towards zero at the desired absorption frequency. Recent advancements in the field of absorption have given rise to three prominent methodologies that significantly influence the physical design and absorption characteristics of metamaterial absorbers at specific frequencies [17]. These methodologies encompass equivalent circuit theory (ECT), standing wave resonance theory (SWRT), and multiple interference theory (MIT). Among them, SWRT has emerged as the most efficacious approach for determining the structural parameters of metamaterial absorber designs [95]. As a result, SWRT serves as the fundamental framework for selecting the structural parameters in the proposed metamaterial absorber. By leveraging the principles of SWRT, the proposed absorber incorporates two metallic layers, situated at the top and bottom, effectively emulating a planar waveguide. This arrangement facilitates the calculation of standing wave modes at the desired frequencies, thus optimizing the absorption performance. [95].

$$S_w = \frac{v}{2D\sqrt{\varepsilon_r}} \tag{1.4}$$

In the given equation, v symbolizes the light velocity in a vacuum, ϵ_r denotes the relative permittivity, and D signifies the electrical length of the resonator at the specific desired frequency. Additionally, it has been noted that the electrical length of each resonator is approximately equivalent to one-fourth of the wavelength, a finding that has been verified and confirmed. through a relationship [95]:

$$L_{eff} = \frac{Le}{\lambda} \tag{1.5}$$

In the given equation, λ represents the wavelength corresponding to the absorption frequency, while *Le* denotes the length of the resonator at the specified frequency. Angular stability is a crucial requirement for metasurfaces, wherein they should maintain their absorptivity at certain angles of TE/TM polarized EM waves. Additionally, metasurfaces need to be polarization insensitive, with the unit cell structure and periodicity determining the stability of polarization angles on the surface. Considering the advantages offered by metasurface absorbers, it is essential to achieve multifunctionality, broadband capability, angular stability, and high efficiency within a single surface. Therefore, the main objective of this thesis is to

8

fabricate, design, analyze, and test metasurface absorbers that can simultaneously provide broad operating bandwidth while maintaining insensitivity to the incidence angle.

1.4   Thesis Organization

This thesis is organized into six chapters, each consisting of multiple sections and subsections. Chapter 2 provides a detailed literature review and comparison of different metasurfaces. It discusses existing research and highlights the strengths and weaknesses of various metasurface designs. In Chapter 3, the design and analysis of the suggested metasurface, capable of absorbing 04x frequency bands, are presented. The fabrication process is also described, and a prototype of the metasurface is created for experimental evaluation. Chapter 4 aims on the design evolution and experimental analysis of a broadband metasurface. The chapter includes experimental results and analysis of the meta surface's performance. In Chapter 5, the design methodology, simulation results, and absorption spectra analysis of a frequency-reconfigurable broadband metasurface are presented. The design approach is described, and the meta surface's ability to change its operating frequency range is demonstrated through simulations. The absorptivity factors are analyzed to evaluate performance of the frequency-reconfigurable metasurface. Finally, Chapter 6 provides a comprehensive conclusion of the thesis, summarizing the key findings and contributions. It also offers future recommendations for further research and development in the field of metasurface design.

CHAPTER 2

Literature Review

Introduction

Metamaterials are artificially designed structures that exhibit unique electromagnetic properties not found in natural materials. They offer a wide range of characteristics, with absorptivity being one of the most recent areas of exploration. Absorptivity refers to the inherent ability of metamaterials to absorb incident electromagnetic waves. The exceptional absorption capabilities of metamaterials, combined with their tunability, simplified design architecture, and near-broadband absorptivity, make them highly suitable for applications in stealth technology.

Metamaterials find utility across various electromagnetic wave spectrums, spanning from optical to microwave and visible frequencies. Their perfect absorption properties and ability to manipulate electromagnetic waves make them particularly well-suited for stealth applications and modules. Unlike naturally occurring materials, metamaterials possess properties that enable them to achieve superior absorption performance. This has led to their increasing significance in various fields.

These properties are not commonly found in natural materials, leading to the widespread acceptance of the metamaterial definition among researchers [18]. Metamaterials are defined as structured materials that simultaneously exhibit negative permittivity and negative permeability [19]. Once these properties are achieved, other variables associated with the material, such as phase velocity (V_ϕ) and wave propagation, are also influenced, including the possibility of backward wave propagation. The inherent properties of metamaterials mentioned above make them highly suitable for a range of applications. Optical cloaking [20], radiation response [21], perfect focusing lenses [22], electromagnetic wave absorption [23], and polarization conversion [24] are just a few areas where metamaterials find utility. Metamaterial absorbers are effective in reducing the radar cross-section (RCS) [25,26], enabling the development of unique metasurfaces for radar stealth and related absorption

applications [26].

The pioneering work on the negative refractive index property of metamaterials dates back to 1968 when Sir Victor G. Veselago first studied it, leading to the exploration of various associated characteristics and a new era in metamaterial research [27]. Subsequently, in 1999, Sir John B. Pendry and his team conducted the first experimental verifications based on Veselago's studies [28]. However, it took some time to develop metamaterials specifically designed for absorption purposes. In 2008, Landy et al. demonstrated electromagnetic wave absorption using metamaterial absorbers with near-perfect absorption [29]. However, it required additional analytical and experimental verifications to establish its validity. Over time, a wide range of metamaterial absorbers with different characteristics have been studied and implemented. These include wideband, ultra-wideband, and polarization-independent absorbers. Metamaterials are available in various forms, such as multi-functional designs [30], polarizers in transmission and reflections [31, 32, 24, 33], circular polarizers in reflection and transmission [34-37], and beam splitters [38]. Within the realm of metamaterial absorbers, a diverse array of options can be found, encompassing single-band, multi-band, and wide-band configurations, and polarization-independent absorbers, all of which have been extensively studied and implemented [39-45]. Researchers have proposed different approaches for metamaterial absorber designs, including passive elements-based designs [46], active elements-based designs [47], and structures incorporating lumped elements [48,49]. Active and lumped-element-based structures offer advantages such as compensating for losses and enhancing bandwidth through negative inductance and capacitance. Nevertheless, these design variations present inherent challenges concerning design complexities, non-linear characteristics, and power-related concerns.

In recent research, the design of metamaterial absorbers has evolved to incorporate various approaches, including single layer metasurfaces, multilayer structures, and cascaded layers, to enhance their applications. These designs have demonstrated effective performance in the GHz and THz frequency ranges. Detailed study of above-mentioned structures is given below: -

2.1   Metamaterial Absorbers – Single Layer

Chetan et al. [50] have devised a metamaterial absorber characterized by a double-squared shape design and implemented with an FR-4 substrate. Their innovative design exhibits wideband absorption capabilities spanning the Ku and K frequency bands, effectively

covering a frequency range from 14.44 GHz to 27.9 GHz. This absorber demonstrates significant potential for applications in radar communication and satellite communication fields, showcasing efficient absorption properties for electromagnetic waves at both normal and varying angles of incidence. In a separate study [51], an absorber based on metamaterial principles was proposed specifically for operation in the low-frequency band, within the 1-2.75 GHz range (L Band). This absorber achieved an impressive absorptivity exceeding 90% within a narrow frequency band, offering utility in 4G communication systems and RFID systems.

Yadgar et al. presented a distinctive swastika-shaped metamaterial resonator in [52], demonstrating effective operation in the X band. This design holds significant applications in the analysis of electrical properties of various chemical liquids, enabling researchers to discern specific characteristics of chemical substances through their electrical properties. Another notable contribution is detailed in [53], where the authors introduced a metamaterial absorber structure employing a single closed-meander wire as a resonator on an FR-4 substrate. This design exhibits absorptivity across multiple frequency bands and remains insensitive to polarization, making it suitable for image sensing and detection applications, especially at wide incidence angles.

In a comprehensive study by the authors in [54], a P-shaped metamaterial absorber resonator was introduced, utilizing two different substrates: FR-4 and Rogers 3035. The design incorporates a spiral-shaped resonator comprising dual and continuous opposite P shapes. The absorptivity of the proposed design spans from 80% to 99.9% in the Ku frequency band (with Rogers substrate) and the K frequency band (with FR-4 substrate). When implemented with an FR-4 substrate, the design functions as a single negative metamaterial absorber within the K frequency band, exhibiting an absorption band from 19.7 GHz to 21.35 GHz. Simultaneously, it operates as a double negative metamaterial absorber within the Ku frequency band, with absorptivity ranging from 15.3 GHz to 17.1 GHz. When utilizing the Rogers 3035 substrate, the same design acts as a single negative metamaterial absorber, effectively absorbing the frequency of 14.65 GHz in the Ku frequency band, and as a double negative refractive index metamaterial absorber within the K frequency band, with an absorptivity range of 18.25 GHz to 16.2 GHz. The design specifically caters to the TEM

mode incidence of electromagnetic waves and exhibits excellent performance for wide incidence angles.

In a separate study by Jafari et al. [55], a Jerusalem cross absorber was proposed, tailored for applications in the X and Ku frequency bands. The design leverages an FR-4 substrate and achieves a substantial absorptivity of 86% across three distinct frequency bands: $f_1 = 8.6$ GHz, $f_2 = 10.3$ GHz, and $f_3 = 11.9$ GHz. Furthermore, the absorber demonstrates reliable performance for oblique incidence angles of up to 60 degrees. In [56], the author presents a microwave absorber design that achieves a wide bandwidth by incorporating an oxide-metal-oxide film in combination with graphene. Monolayer graphene is grown on a graphene frequency selective surface (FSS) through chemical vapor deposition, effectively reducing the sheet resistance to 150 Ohms/square via HNO_3 doping. This design finds diverse applications in radar stealth surfaces and other electromagnetic wave-compatible systems.

Another significant contribution discussed in [57] is a triple-band absorber design showcasing three absorption peaks at $f_1 = 3.5$ GHz, $f_2 = 6.35$ GHz, and $f_3 = 11.5$ GHz, achieved through a unit cell configuration. The proposed structure achieves absorptivity exceeding 90% and remains insensitive to both transverse electric (TE) and transverse magnetic (TM) modes of incident waves. This design finds broad applications in microwave and X-band absorption surfaces. In [58], a wideband metamaterial absorber with a two-squared-shaped design was proposed by Ranjan et al. The absorber, fabricated using an FR-4 substrate, achieved wideband absorption spanning 6 GHz (5.9 GHz to 11.9 GHz) with a full-width at half-maximum (FWHM) bandwidth of 7.5 GHz within the range of 5.5 GHz to 13.1 GHz. The design exhibits nearly unity absorption peak and remains unperturbed by polarization or oblique incidence angles, making it suitable for applications within the X frequency band spectrum. In a study by Zhou et al. [59], an ultra-thin metamaterial absorber employing a double-squared loop structure was designed. The absorber, utilizing an FR-4 substrate as the dielectric material, achieves maximum absorption at a frequency of 6.75 GHz, resulting in a reduction of the radar cross-section (RCS) by up to 14.9 dB, thus providing applicability in radar stealth materials. Guang Sheng Deng et al. [60] proposed an ultra-thin triple-band metamaterial absorber based on a polyimide substrate and structured metamaterial absorber elements. The absorber effectively absorbs three distinct frequency peaks at 8.5 GHz, 13.5 GHz, and 17 GHz, exhibiting absorptivity surpassing 89%. This

design demonstrates polarization insensitivity and remains effective for various polarization incidence angles, finding applications within the X and Ku frequency bands. Saif Hannan et al. [61] presented an absorber design based on two Split ring resonators (SRRs). The design was verified using equivalent circuit analysis, enabling the design of co-polarization insensitive metamaterial absorbers without relying on lumped circuit elements. By incorporating a frequency selective surface (FSS), the absorber achieved two absorption peaks at 2.5 GHz and 5 GHz, resulting in perfect absorption of Wi-Fi signals. In [62], Jie Qian et al. proposed a Hybrid metamaterial absorber (HMM) based on a metal/insulator/metal (MIM) design utilizing permalloy. The design was evaluated on PET and glass substrates, demonstrating near-perfect absorption in the frequency band of 7.1 GHz. The proposed structure allows for the absorption of microwave signals, generating DC current based on spin rectification. The design finds applications in opto-spintronics, magnonic metamaterials, and wireless energy transfer. Javad Shabanpour et al. [63] introduced a reconfigurable metamaterial absorber (MMA) based on honeycomb and VO2 films. The design exhibits the highest-ever proposed absorptivity exceeding 90% at incident angles up to 87°. The MMA remains polarization insensitive and achieves absorptivity within the frequency band of 1 THz to 4 THz, finding applications in camouflage, electromagnetic interference, imaging, and sensing. In [64], the authors proposed a wideband metamaterial absorber employing a metallic patch and FR-4 substrate with a thickness of 1.578 mm. Due to its C4 symmetric design, the absorber remains insensitive to polarization angles up to 45°, exhibiting absorption of over 90% within the X and Ku bands at frequencies of 11.31 GHz, 14.11 GHz, 14.23 GHz, and 17.79 GHz. It finds numerous applications in stealth technology. Yan-Lin Liao et al. [65] presented an ultra-narrowband dielectric metamaterial absorber based on ultra-sparse dielectric nanowire grids. The design utilizes gold as the substrate material and silicon for the nanowire grid. Through rigorous coupled wave analysis (RCWA), the absorber achieves an absorption peak of 99% at a wavelength of λ = 1.48251 µm. The absorption spectrum was studied for varying refractive indexes, demonstrating ultra sensitivity of 1052 nm/RIU and a large figure of merit (FOM) of 2768. In [66], the author proposed a wideband metamaterial absorber based on concentric crossed eclipses. The model utilizes a metal-dielectric-metal (MIM) structure to maximize the absorption of infrared (IR) radiation. The design incorporates gold and TiO2 metallic split-ring resonators (SRRs), with cuts in the SRRs acting as diodes for current rectification. The proposed design achieves

14

absorption within the frequency range of 30 THz, making it suitable for energy harvesting applications.

2.2   Multi-Layer Metamaterial Absorbers

In [67], Mehmat et al. proposed a wideband metamaterial absorber based on split ring resonators (SRRs). The design achieved near-perfect absorption in the frequency range of 4 GHz to 16 GHz, making it suitable for applications in energy harvesting. In [68], the authors presented an ultra-thin metamaterial absorber with three absorption peaks at frequencies f1=3.4 GHz, f2=6.4 GHz, and f3=11.5 GHz. The absorber exhibited triple-band absorption in the range of 3 GHz to 11 GHz, and it was polarization-insensitive and capable of operating at oblique angles up to 45˚. Potential applications include microwave and X-frequency bands. In [69], a broadband metamaterial absorber was designed to achieve over 90% absorptivity across a wide frequency range from 0.95 GHz to 18.5 GHz. The absorber utilized double layers of resistive films and eight square patches with a double ring structure. It demonstrated insensitivity to polarization angles, making it suitable for various applications. Jiakun et al. [70] proposed a graphene capacitor-based tunable radar absorber metasurface. By manipulating the effective sheet resistance of the graphene capacitor, the absorber demonstrated the ability to attain absorption across a broad frequency spectrum spanning from 2.9 GHz to 16 GHz. It was insensitive to polarization angles and exhibited angular stability, making it applicable in radar stealth applications. In [71], a dual-band polarization-insensitive metamaterial absorber based on split ring resonators (SRRs) and an inner cross conductor was proposed. The absorber achieved 90% absorptivity with a bandwidth of 400 MHz from 21.4 GHz to 21.8 GHz, and an additional 760 MHz bandwidth from 23.84 GHz to 24.24 GHz. It remained polarization-insensitive up to a 90˚ incidence angle and found applications in pressure sensing technology. Xiaoming Liu et al. [72] presented a two-band metamaterial absorber based on a structured dielectric molecule. The design provided double absorption peaks at 9.4 GHz and 11.7 GHz, and it remained polarization-insensitive up to 75˚ incidence angles. The absorber had applications in detectors, transceiver systems, and spectroscopy imaging. In [73], A novel concept of a dual-layered metamaterial absorber-based camera with subwavelength spatial resolution was introduced. The design utilized a front metal structure with RLC resonators, a dielectric substrate, and a metallic plate at the back. The camera exhibited little far-field distortion and had applications in subwavelength imaging systems, non-destructive detections, and beam directional tracers. Lincy Stephen et

al. [74] proposed a bandwidth-enhanced bidirectional metamaterial absorber based on strips and squares. The absorber achieved 90% absorptivity in the frequency range of 13.4 GHz to 14.25 GHz. It utilized a front model of strips and squares, and a metallic back plate (copper) with an FR4 dielectric substrate. The final design obtained absorptivity from both sides and exhibited C4 symmetry. In [75], the author proposed a soil moisture-based perfect metamaterial absorber (PMA) with 100% absorptivity for electromagnetic waves. The design used a squared shaped waveguide with perpendicular slots etched into the borders to detect water content in the soil. It found applications in soil moisture sensor devices. In [76], a pyramidal metamaterial absorber based on a real pillbox cavity was proposed. The design achieved wideband absorption by uniting multiple layers with different absorption peaks. By optimizing the substrate thickness, absorption peaks at 3 & 4 GHz were obtained. The absorber worked as a accurate mode dampener in a pillbox microwave testing environment. Keng-Te Lin et al. [77] proposed a 3D structured graphene metamaterial (SGM) absorber for almost 100% absorptivity of solar thermal radiation. The design consisted of multiple layers, including a top layer of graphene, a dielectric layer, another graphene layer, and a metallic plate at the bottom with vertical stacking of dielectric slots at the edges. The absorber used photothermal radiation absorption and was capable of selective and broadband absorption of solar radiation. It exhibited insensitivity to the polarization of incidence light and had applications in solar energy harvesting. In [78], the author proposed a fractal periodic resonator structure for a metamaterial absorber. The design consisted of four elliptical ring-shaped resonators internally connected to form a fractal structure. Tungsten was used as the material on a dielectric substrate (silicon diode), and a copper plate served as the back. The proposed fractal metamaterial absorber achieved over 90% absorptivity against incident light at all angles in the wavelength range of 400 nm to 750 nm. The design was verified using the Fabry-Pérot model.

2.3   Metamaterial Absorbers using Lumped Elements

In [79], a metamaterial absorber design based on squared loops was proposed. These squared loops, acting as resistive loaded components, functioned as frequency-selective surfaces (FSS) resistant to the overall coupling environment. By combining resistive resonant squared loops (RRSL) with distinct geometric configurations on a single layer of dielectric substrate, the design achieved wide absorption bandwidth from 7.9 GHz to 18.9 GHz (overall bandwidth of 11 GHz) with an absorption rate of over 86%. In [80], a resistive film and

16

glass-based metamaterial absorber unit cell design was introduced. This design was insensitive to the polarization of incident waves and achieved wideband absorption of 15 GHz (3.5 GHz to 18.5 GHz). It found applications in stealth radar technology and electromagnetic wave shielding. In [81], Guo et al. proposed a stretching transformation-based metamaterial absorber. The design included a dielectric layer, variable capacitor, and metal patch-based loading resistor. The variable capacitor provided tunability to the loading resistor, resulting in a narrow bandwidth of 1.4 GHz ranging from 0.7 GHz to 2.1 GHz. In [82], an antique-type metamaterial absorber using active components was proposed. This design could absorb the entire X-band and Ku frequency band using lumped resistors. It exhibited angular stability for different incidence angles of electromagnetic waves (both TE and TM modes) and was insensitive to the incidence angle. In [83], authors proposed a unit cell-based metamaterial absorber design providing absorptivity of up to 90% from 4 to 10.5 GHz. The design utilized four loaded SMT resistors to enhance the absorption range. It had a symmetrical design architecture with circles and slotted sectors, resulting in insensitivity to polarization angles. In [84], a low-profile absorber (LPA) design achieved wideband absorption of a 9 GHz frequency band (3 GHz to 12 GHz). It utilized a lossy capacitive surface and metallic ground to provide total reflectivity from the ground, thereby achieving total absorptivity by the capacitive surface-based metamaterial absorber. The design demonstrated insensitivity to the polarization of incident waves, making it polarization-independent and suitable for bi-stealth applications. In [85], the proposed design used eight lumped resistive elements with a value of 250 ohms each. Based on frequency-selective surfaces (FSS), this metamaterial absorber had a wide frequency band absorption of 6 GHz, ranging from 8 GHz to 13.4 GHz. It could be implemented with various polarization angles up to 60˚ and exhibited insensitivity to the polarization of electromagnetic waves due to its C4 symmetry. In [86], a metamaterial absorber design based on two weakly coupled layers was proposed. The weak coupling resulted in frequency-selective bands, where the center layer acted as the frequency-selective surface (FSS) and the coupling between the outer layer and the FSS layer was weak, leading to different frequency-selective absorption bands. This design achieved wideband absorption in the frequency range of 13 GHz (2.9 GHz to 16.65 GHz). In [87], a metamaterial absorber structure based on metal wire arrays with a frequency-selective surface phenomenon was proposed. This design provided a wideband absorptivity of 11 GHz, ranging from 8 GHz to 19.5 GHz, making it suitable for stealth applications. It

17

exhibited absorption rates above 90% for all incidence polarization angles up to 70 degrees, making it polarization independent. In [88], an ultra-broadband metamaterial absorber with multiple absorption peaks ranging from 7 GHz to 16.5 GHz was proposed. This tunable multilayer metamaterial absorber (TMA) used lumped elements, making it an active metamaterial absorber. The design included a continuous metallic plane with three split-ring resonators (square-shaped) imposed on it, sandwiching a dielectric layer. The substrate contained Y-shaped solid-state plasma resonators and truncated ring-shaped resonators. The structure was tested for various polarization incidence waves and found to be polarization-independent for electromagnetic waves. In [89], Cuilian Xu et al. proposed a hybrid metamaterial absorber (HMA) for infrared-multiband bi-stealth applications. The design comprised two structures separated by a foam surface: an infrared shielding layer (IRSL) consisting of metallic squared patch arrays providing low infrared emissivity, and a radar absorption layer (RAL) used to absorb X-band frequencies, comprising four L-shaped metallic resonators. The two layers utilized different dielectric constants (F4B and FR4) and were separated by a foam layer of defined thickness. This design was suitable for IR-radar bi-stealth applications and exhibited five strong absorption peaks at 6.35, 8.38, 12.1, 15.37, and 18.05 Gigahertz, respectively. In [90], Heijun Jeong proposed a thin electric metamaterial absorber using four inductive lumped elements on a square loop resonator. This design introduced polarization angle insensitivity through a simpler design with 90° rotational symmetry. The model utilized a square-shaped resonator with a chip inductor and an FR4 substrate, achieving wideband absorption at 2.4 GHz with a small error of 1.2%. The model had applications in ultra-low-frequency absorption and acoustic applications.

2.4   Metasurfaces in THz Frequency Regime

Within the electromagnetic spectrum, the terahertz (THz) frequency range, encompassing frequencies from 300 GHz to 3 THz, having numerous applications, particularly in biochemical and pharmaceutical sciences. Metasurfaces designed to operate within this frequency range have been explored in the literature, showcasing the development of cross- and circular-polarizers [91-93]. While THz devices based on cross-polarization converters generally exhibit lower efficiency, one specific design stands out as a high-efficiency terahertz device [91]. The proposed design involves C-shaped gold antennas supported by gold gratings at the bottom. Fig. 2.1 provides a comprehensive representation of the numerical, theoretical, and experimental calculations of the meta surface's transmission,

demonstrating an efficiency exceeding 85% across the desired bandwidth.
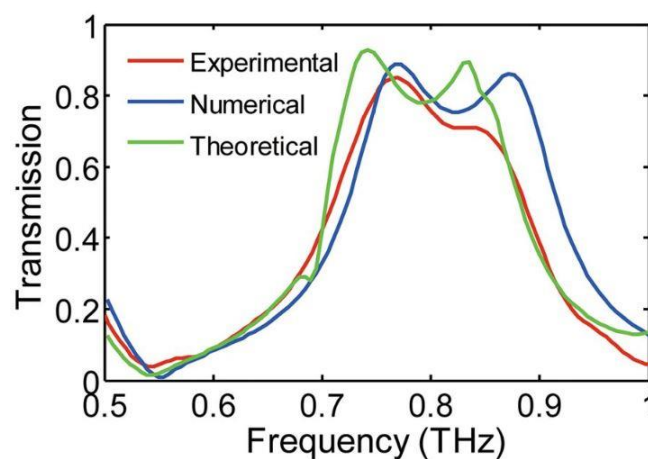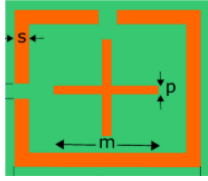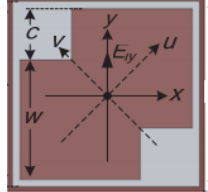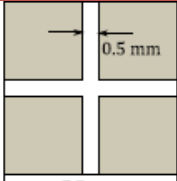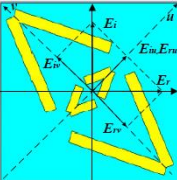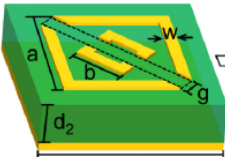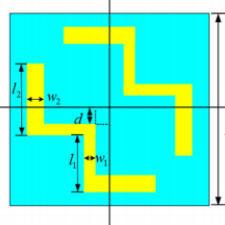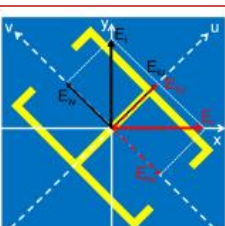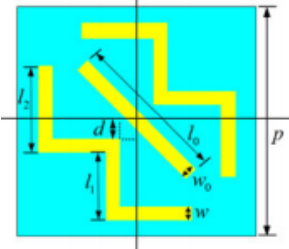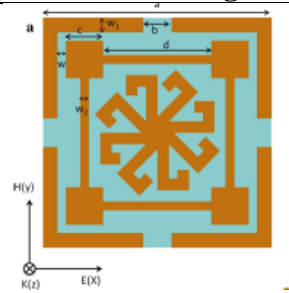
Figure 2.1: Transmission coefficient of experimental, numerical, and theoretical results of the designed

metasurface [91]
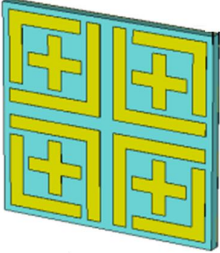
A novel approach to achieving wide-view circular polarizers is introduced, offering a significant advancement in the field. The authors have developed a methodology for creating single and broadband wide-view circular polarizers that operate within a range of ±85˚ [93]. In this innovative metasurface design, the optical efficiency has been significantly improved, leading to enhanced performance and functionality.
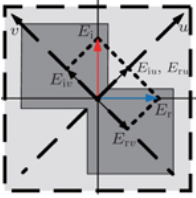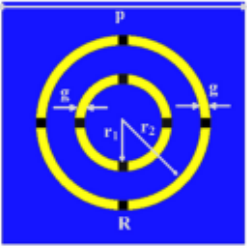
To highlight the importance of meta surfaces w.r.t their angular stability, polarization insensitivity and their efficacy a comprehensive analysis of different designs have been carried out in detail based on their absorption band, limitations and designing methodology. Table below contains the comprehensive analysis of few designs with have been counted in in the literature review:
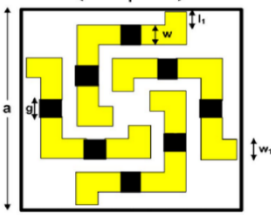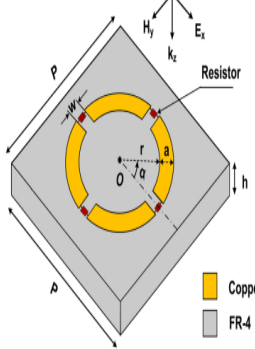
Table 1: Evaluation of Metasurfaces based on operations and limitations.

Research Paper	Unit Cell	Operation	Bandwidth	Limitations
Scientific Reports (2017)		Quarter-Wave plate and half mirror	24.6-26.6 GHz	Narrowband Operation
Progress In Electromagnetics Research (2018)		Circular-Polarizer Half-wave plate operation	7.6-11.2 GHz	Single Operation, Narrowband

19

Paper	Unit Cell Design	Technique	Pros	Cons
TAP-(2018)		Half-wave plate operation	8.5-11.56 GHz	Normal incidence, multi-layered
J. Appl. Phys (2018)		Half-wave plate operation	14.2-43.2 GHz	Single Operation
Optics Express (2018)		Half-wave plate operation	6.7-17.1 GHz	Low efficiency, single operation
Journal of ELECTRONIC MATERIALS (2018)		Cross Polarizer	8.40 GHz to 20.15 GHz	Limited angular stability
Optics Express (2018)		Cross Polarizer	7 to 19.5 GHz	Angular Stability up to 41.5 degree
IEEE AWPL (2019)		Cross Polarizer & Circular polarizer	6.53 to 12.07 GHz (HWP) 13.70 to 15.60 GHz (QWP)	Normal Incidence
Paper	**Unit Cell Design**	**Technique**	**Pros**	**Cons**
An Ultrathin, Triple-Band Metamaterial Absorber with wide Angular Stability at X and Ku Frequency Bands (Guang sheng Deng		• **Absorption** • Said paper propose triple absorption peaks (8.5, 13.5, 17 GHz) using ultrathin metamaterial absorber (MA)	• X and Ku band absorption at 3x peaks (8.5, 13.5, 17 GHz) achieved with approx. 89% accuracy • Insensitivity to angle of	• Use of polyimide substrate is not cost effective. • Not lossy material used as per most of the

20

Paper	Unit Cell Design	Technique	Pros	Cons
et al, "An Ultrathin, Triple-Band Metamaterial Absorber with Wide-Incident-Angle Stability for Conformal Applications at X and Ku Frequency Band", research letters, 2020).		using polyimide substrate. • X and Ku band absorption • Author uses symmetric geometry concept to achieve C4 absorption. • Linearly polarized incident waves have been absorbed with zero or minimum reflection	incident up till 60 degrees • No effect on absorption scale using different polarization angles. • Thin material having flexibility to be used for implantation on any surface	today applications. • No band absorption only 3x peaks absorptivity achieved
"Hybrid metasurfaces for infrared-multiband radar stealth-compatible applications" (Cuilian Xu, "Hybrid metasurfaces for infrared-multiband radar stealth-compatible materials applications", IEEE Access, 2020)		• **Absorption** • The designed MA has been proposed for radar stealth compatible materials. • Said paper proposes use of 2x layers, one each for IRSL (infrared radar Stealth layer) and RAL (radar absorption layer) respectively. • It uses different types of material, namely cupper and F4B of varying thicknesses for development of IR stealth	• Five absorption peaks have been achieved at 6.35, 8.38, 12.10, 15.37 and 18.05. • 89% max absorption has been achieved using x-polarized wave incident experiment at max 45-degree angle of incidence.	• Absorptivity varies with incident angle of more than 45 degrees. • Absorptivity sharply varies once two layers are combined. • *This metasurface operates only for normal incidence angle.* • More complex design

Paper	Unit Cell Design	Technique	Pros	Cons
		and radar wave absorption.		
Metasurfaces with Half-wave Plate Operation **Ultra-wideband Cross-pol** (W. Jia-Liang, L. B. Qin, and D. Xin-Yu, "Ultra-wideband reflective polarization converter based on anisotropic metasurface," *Chinese Physics B,* vol. 25, p. 088101, 2016.)		• **Polarization conversion** • One of the most widely used techniques to get broadband cross polarization is *multiple plasmonic resonances.* The novel anisotropic unit cell configuration of double-head arrow produces four plasmon resonances which has made it ultra-wideband	• Bandwidth of 13 GHz has been achieved in the frequency range of 7.57 GHz to 20.46 GHz. • The Experimental and simulated results are in parallel with each other that makes this metasurface strong candidate for polarization conversion applications for normal incidence only.	• *This metasurface operates only for normal incidence angle*. • Only for linearly polarized light • Complex design • Useful only for normal incidence wave
S. Sambhav, J. Ghosh, A. K. Singh, **"Ultra-Wideband Polarization Insensitive Thin Absorber Based on Resistive Concentric Circular Rings"** IEEE Transactions on Electromagnetic combability (2021)		• **Absorption** • Said paper propose a broad band absorber ranging from (6.7-20.58 GHz) using FR-4 substrate. • X, Ku and K band absorption • Author uses symmetric geometry concept to achieve C4 absorption.	• Covering wide range of absorption range • Insensitivity to angle of incident up to 90 degrees. • No effect on absorption scale using different polarization angles.	• Although the design has been made on FR-4 lossy substrate and has C-4 symmetry, it lacks angular stability. Number of SMT resistors used are large in numbers which ultimately makes it less cost effective.

Paper	Unit Cell Design	Technique	Pros	Cons
Pathak Tiwari, Surya. K. Pathak, and V. Siju. "**Design, development and characterization of resistive arm based planar and conformal. metasurfaces for RCS reduction**," Scientific Reports (2022).		• **Absorption** • Said paper propose a broad band absorber ranging from (13.42-22.66 GHz) using ultrathin metamaterial absorber (MA) using FR-4 substrate. • Ku and K band absorption • The author uses symmetric geometry concept to achieve C4 absorption.	• K and Ku band wide absorption ranging from (13.42-22.66 GHz) achieved with approx. 95% accuracy • Insensitivity to angle of incident up till 90 degrees. • No effect on absorption scale using different polarization angles. • Thin material having flexibility to be used for implantation on any surface.	• Although the design has been made on FR-4 lossy substrate and has C-4 symmetry, it lacks angular stability. • Number of SMT resistors used are large in numbers which ultimately makes it less cost effective.
T.Q.H. Nguyen, T.K.T. Nguyen, T. N. Cao, H. Nguyen and L. G. Bach "**Numerical study of a broadband metamaterial absorber using a single split circle ring and lumped resistors for X-band applications**" AIP Advances (2020)		• **Absorption** • Said paper propose a broad band absorber ranging from (7.8-12.6 GHz) using FR-4 substrate. • X and Ku band absorption • The author uses symmetric geometry concept to achieve C-4 absorption.	• The design has good polarization insensitivity up to 90 degrees. • The meta surface was designed on cost-effective FR-4 substrate and have applications in EM shielding	• The designs lack angular stability. • Having much greater substrate thickness

23

2.5   Summary

The literature mentioned above explores cutting-edge designs of metasurface absorbers, highlighting their various functionalities such as angular stability, polarization insensitivity, and absorption mechanisms. This research on metamaterial absorbers offers valuable insights into developing absorbers that are more efficient and cost-effective for specific applications. Moreover, it has the potential to advance metamaterial design, enabling the creation of highly effective absorbers for diverse application areas. Therefore, investigating metamaterial absorbers is a valuable research area that can propel the development of more efficient and effective absorbers across various applications. The literature review conducted in this thesis examines several key challenges that form the basis of this research. The following paragraphs discuss some of these core challenges identified through the review, which have influenced the foundation of this thesis.

- **Bandwidth limitation**: Achieving a broad operational bandwidth is a challenge due to the inherent resonances and narrowband response of traditional metamaterial structures.

- **Polarization sensitivity**: Ensuring polarization insensitivity is crucial for practical applications. Designing a metamaterial that exhibits consistent performance irrespective of the incident polarization is a challenge. Therefore, the design must have C-4 symmetry.

- **Angular stability**: Another challenge is the maintenance of angular stability over wide frequency range. The metamaterial should exhibit similar absorption characteristics regardless of the angle of incidence.

- **Frequency tunability**: Designing a metamaterial that can be tuned to operate at different frequencies is a significant challenge. This involves controlling the resonance response and achieving frequency tunability while maintaining other desirable properties.

- **Material selection**: Choosing suitable materials with appropriate electromagnetic properties that can effectively manipulate the incident waves over a broad frequency range is challenging. Identifying materials with low losses and high tunability is critical. In our case selection of FR-4 substrate is considered.

- **Fabrication complexity**: The fabrication process for C4 symmetric broadband and

frequency tunable metamaterials can be complex. Ensuring precise control and replication of the desired structure at the nanoscale or microscale can pose challenges.

- **Cost-effectiveness**: Balancing the performance requirements with cost considerations is an ongoing challenge. Developing cost-effective fabrication techniques and utilizing materials that are readily available can contribute to addressing this challenge.

2.6   Problem Statement

To address the limitations observed in current metasurface absorbers, such as limited absorption peaks (3 to 4), low angular stability (up to 45˚ to 50˚), limited polarization insensitivity (up to 60˚ to 70˚), and relatively low absorptivity (up to 90%), we propose the development of a multi-band metamaterial absorber. This absorber would exhibit enhanced angular stability ($\geq$ 60˚) and insensitivity to polarization ($\geq$ 90˚). Additionally, we have designed and fabricated the tetra-band and broadband metamaterials capable of covering a wide frequency range, while maintaining excellent angular stability, polarization insensitivity, and achieving absorption levels exceeding 99%. By focusing on these improvements, we aim to overcome the existing limitations and provide advanced metamaterial solutions for various applications.

CHAPTER 3

Novel, highly efficient, and insensitive to polarization tetra band metamaterial absorber on a thin substrate.

Introduction

This chapter introduces a brand-new multipurpose metasurface absorber that can achieve flawless absorption in the C, X, and Ku frequency bands. This metasurface completes all the functionalities simultaneously within a single-layered structure, in contrast to existing designs in the literature that achieve separate operations, such as broadband absorption, angular stability, and polarization insensitivity, using complex structures and multiple layers. Wider bandwidth, high efficiency, and angular stability are made possible by the suggested unit cell design and geometric configurations, removing the constraints imposed by production methods and practical application. The distinct metasurface arrangement has a great deal of promise for use in many different electromagnetic applications. This chapter introduces a novel metamaterial absorber (MA) design that is symmetrical, single-layered, highly efficient, and capable of wide-angle and polarization-stable absorption. The absorber is fabricated on a thin dielectric layer with a thickness of 0.8 mm and exhibits four distinct absorption peaks. The compact geometry of the MA is achieved by combining two circular rings with a square-shaped arrangement of four split ring resonators (RR), along with a circular patch and a square ring in each unit cell. This arrangement enables mutual coupling between the elements, creating an independent environment that enhances performance. The proposed MA demonstrates polarization insensitivity over wide incident angles for both transverse electric (TE) and transverse magnetic (TM) waves at four frequency bands: 7.16 GHz, 10.175 GHz, 12.92 GHz, and 16.82 GHz, with absorptivity values of 99.6%, 97.2%, 98.3%, and 94.8%, respectively. The experimental validation of the prototype was conducted in an anechoic chamber to verify the simulated results.

The chapter is structured as follows: In section 3.1, the geometrical layout and design evolution of the proposed structure are presented. section 3.2 provides a comprehensive analysis of the design evolution process. The Absorption Characteristics of the Frequency Spectra is discussed in section 3.3, while section 3.4 focuses on the distribution of the surface current. Section 3.5 Authentication of the meta material nature of the Proposed MA unit cell, section 3.6 describes the Electric field analysis. Experimental verification is explained in section 3.7 and finally the chapter's concluding remarks are in section 3.8.

3.1   Methodology of Design and its Evolution

3.1.1   Geometrical Configuration layout of the Unit Cell

Figure 3.1 (a) presents an illustrative representation of the geometric dimensions of the finalized unit cell. The uppermost layer of the unit cell showcases four distinct conducting patterns. For the absorption resonant peaks at 7.26 GHz and 10.24 GHz, two separate circular rings are incorporated. A rectangular split ring resonator (SRR) with symmetrical splits is introduced as the third independent structure, chosen for its suitability for miniaturization, to achieve absorption at 12.77 GHz. Additionally, a square-shaped strip coupled with a circular patch act as the fourth resonator, resulting in absorption at 16.90 GHz. The unit cell employs a thin dielectric substrate of 0.8 mm thickness made of FR-4 material, featuring a relative permittivity (ϵ_r) of 4.3 and a loss tangent (tan δ) of 0.025 in the middle layer. The ground layer is composed of copper with a thickness of 0.02 mm, exhibiting an electrical conductivity of 5.8×107 S/m. The design modeling, analysis, and optimization processes are conducted using CST Microwave Studio 2019. Finite boundary conditions are applied along the x and y directions, while plain wave excitation is introduced from the z-axis using Floquet ports. Figure 2.1 (b) illustrates the final optimized dimensions of the proposed unit cell and provides an overview of its structural anatomy. Further details regarding the design evolution of the unit cell, as well as the functionality of each included conducting pattern, will be discussed extensively in the subsequent subsection.
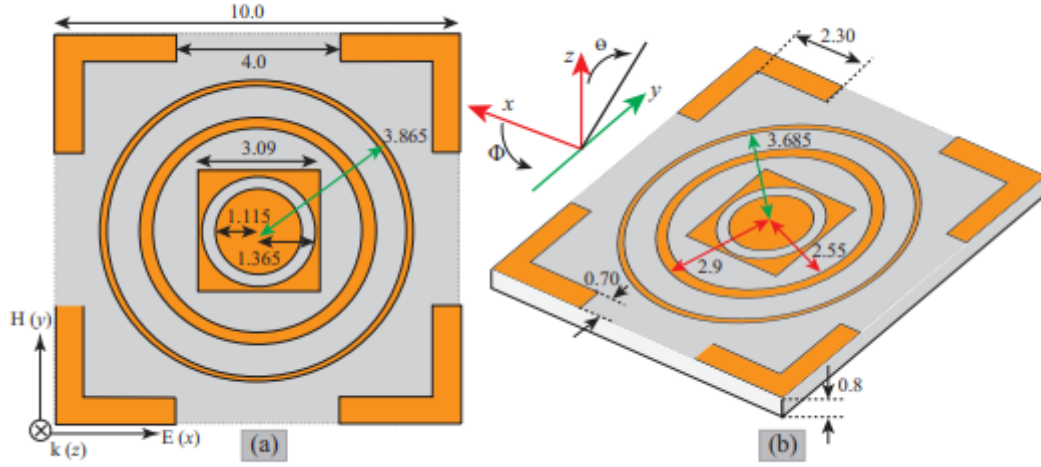
Figure 3.1: Layout of the unit cell (a) Upper view (b) Isometrical View.

3.2 Progression of Design and Functionalities of Integrated Structures

In pursuit of wide-angle polarization insensitivity, angular stability, and multiband absorbance, the initial iteration of the design focused on incorporating two circular ring geometries. The utilization of circular ring structures was favored due to their circular symmetry and inherent polarization insensitivity. To ensure a single resonance and avoid the occurrence of weak resonances, the electrical length of the circumference of the two circular rings was carefully set to be one wavelength long at frequencies of 7.26 GHz and 10.24 GHz, respectively. Mathematically, circular rings resonance is given by:

$$C = \sqrt{\varepsilon_{eff}} = \lambda \tag{3.1}$$

The circumference of the corresponding circular rings, denoted as C, and the effective permittivity of the dielectric substrate, represented as ε_{eff} play crucial roles in the design. By utilizing the wavelength λ, which can be calculated using the equation v = f λ, the resonance frequency can be determined. A 0.8 mm thick FR-4 substrate with a relative permittivity (ε_r) of 4.3 and a loss tangent (tan δ) of 0.025 was chosen due to its cost-efficacy (economical) and widespread commercial accessibility.

To determine the radii of the circular rings within the X band, equation (3.1) was employed. For the frequencies of 7.26 GHz and 10.24 GHz, circular rings with widths of 0.18 mm and 0.35 mm, respectively, were chosen. These radii were then implemented in the CST simulation software, where the circular rings were modeled on the upper layer of the 0.8 mm FR-4 substrate, while a solid ground plane was modeled on the bottom of the substrate. Copper with a thickness of 20 µm was used as the conductor material in the design. The absorptivity of the included circular rings is then studied by plotting the absorption coefficient from the given equation:

$$A(\omega) = 1 - |S_{11}(\omega)|^2 - |S_{21}(\omega)|^2 \tag{3.2}$$

The reflectivity coefficient ($S_{11}(\omega)$) and transmittivity coefficient ($S_{21}(\omega)$) are utilized to characterize the performance of the design. In the presence of a ground plane, the transmission coefficient ($S_{21}(\omega)$) tends to approach zero. However, due to a strong resonance and the effects of electrical and magnetic losses that trap traveling waves, a robust absorption mechanism is established at the resonant frequencies. The absorption resulting from the incorporation of circular rings is visually represented in Figure 3.2. Subsequently, a rectangular resonator is chosen as the second independent geometric structure. The implementation of rectangular shapes offers advantages in terms of miniaturization and dense packing, while maintaining the overall dimensions of the unit cell. To achieve a higher resonant value compared to a single conventional split ring resonator (SRR), the SRR is modified with four splits. The inclusion of these additional gaps in the structure reduces the overall capacitance while simultaneously increasing the magnetic resonance frequency ($\omega_m^2 = 1/(LC)$). Consequently, the second iteration of the four-split SRR leads to resonance at 12.77 GHz. The absorption peak resulting from the incorporation of the four-split SRR is depicted in Fig. 3.2. To achieve the fourth resonance, a combination of a circular patch and a rectangular strip is employed. The introduction of these two structures creates a tight coupling effect, which contributes to the emergence of a resonance peak at 16.90 GHz. The impact of incorporating these new structures can be observed in Fig.3.2, where a distinct fourth absorption peak resulting from the fourth conductive pattern becomes apparent.

The inclusion of the rectangular strip, along with the circular patch, serves multiple purposes. Not only does it shield the capacitive couplings from the circular rings, but it also aids in establishing independent structures with their own resonance peaks. This approach allows for the achievement of distinct resonances and enhances the overall performance of the metamaterial absorber.
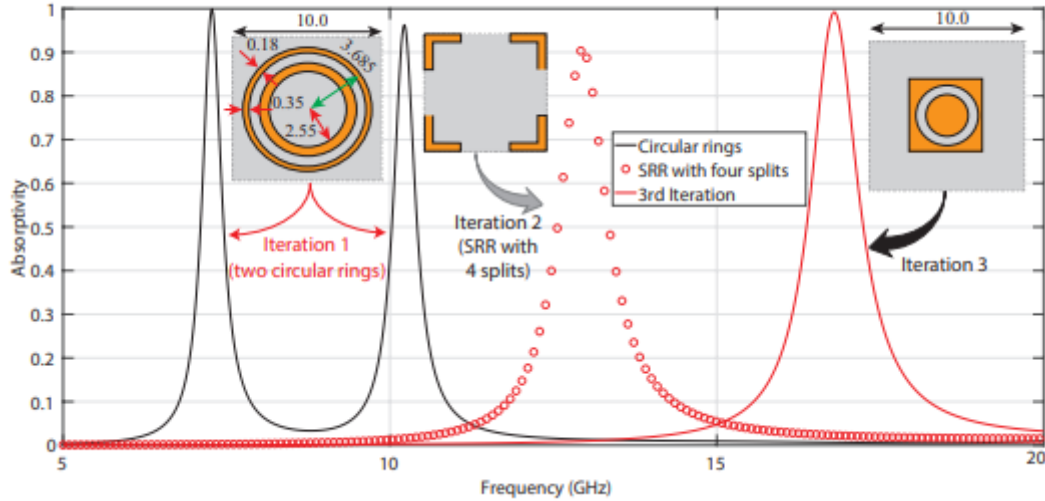
Figure 3.2: Progression of Design of the MA unit cell.

To achieve comprehensive design advancement, the principles of Standing Wave theory (SWR) were employed, serving as the cornerstone for meticulously selecting the dimensional structural parameters to enable absorption at the desired frequency, as depicted in Figure 3.1. To accurately calculate the standing wave mode, the following mathematical expression will be employed. Given that our proposed metamaterial absorber design consists of both upper and lower metallic layers, it can be effectively treated as a planar waveguide.

$$S_w = \frac{v}{2w\sqrt{\varepsilon_r}} \tag{3.3}$$

The relative permittivity of the substrate, denoted as ε_r and the speed of light in a vacuum, represented by v, play significant roles in the following analysis. Specifically, the length of the assigned resonator at a given absorption peak frequency is represented by w. By substituting w = 4.32 mm into Equation (3.3), we obtain a calculated frequency, f, of 16.744 GHz, which closely aligns with the observed absorption peak at 16.88 GHz. This absorption peak corresponds to the inner square structure within our proposed metamaterial absorber unit, which is surrounded by a circular ring.

Furthermore, it is worth noting that the approximate electrical length of each resonator, denoted as λ/4, has been verified using the relationship $L_{eff} = \frac{w}{\lambda}$, where λ represents the wavelength corresponding to the absorption peak frequency. As an example, when w = 4.32 mm, the electrical length of the inner square structure with the circular ring is λ/4. This validation ensures that the electrical lengths of all other elements utilized in the design are approximately equal to λ/4, as determined by the expression. Consequently, this confirms the compact size of our designed metamaterial absorber unit. Moreover, our designed metamaterial absorber exhibits a mere substrate thickness of 0.8 mm, further emphasizing its sub-wavelength dimensions. This is reinforced by the effective wavelength of $0.019\lambda_o$ at 7.16 GHz and $0.044\lambda_o$ at 16.82 GHz, indicating that the size of our proposed metamaterial absorber is significantly smaller than the corresponding free-space wavelength (λ_o).

3.3 Absorption Characteristics of the Frequency Spectra

The absorption characteristics of the individual conductive patterns integrated into the unit cell are depicted in Fig. 3.3. This figure clearly demonstrates that the incorporated metamaterial structures are responsible for four distinct and independent absorption peaks. A minimal shift observed in the resonant peaks of the unit cell, compared with the individual structures, validates the independent nature of the proposed design. Furthermore, the consistent absorption characteristics for both transverse electric (TE) and transverse magnetic (TM) polarized waves confirm that the circular and four-split SRR structures exhibit cyclic (C-4) symmetrical layouts. The compact arrangement of the circular rings, circular patch, and four-split ring resonators within the proposed unit cell results in a significant reflective area. This, in turn, contributes to the generation of high absorption peaks even when the structure is rotated, as evidenced by the variation in θ. Additionally, the proposed structure exhibits polarization insensitivity, with 90% absorptivity observed across various angles (φ) of incidence, as shown in Fig. 3.4. This observation holds true for both TE and TM polarized waves. The absorption peaks also remain stable at higher angles of incidence in the θ plane, as indicated by Fig. 3.4. In summary, the absorption characteristics analysis highlights the independent behavior of the integrated conductive patterns, the cyclic symmetry exhibited by certain structures, and the polarization insensitivity of the proposed metamaterial design.
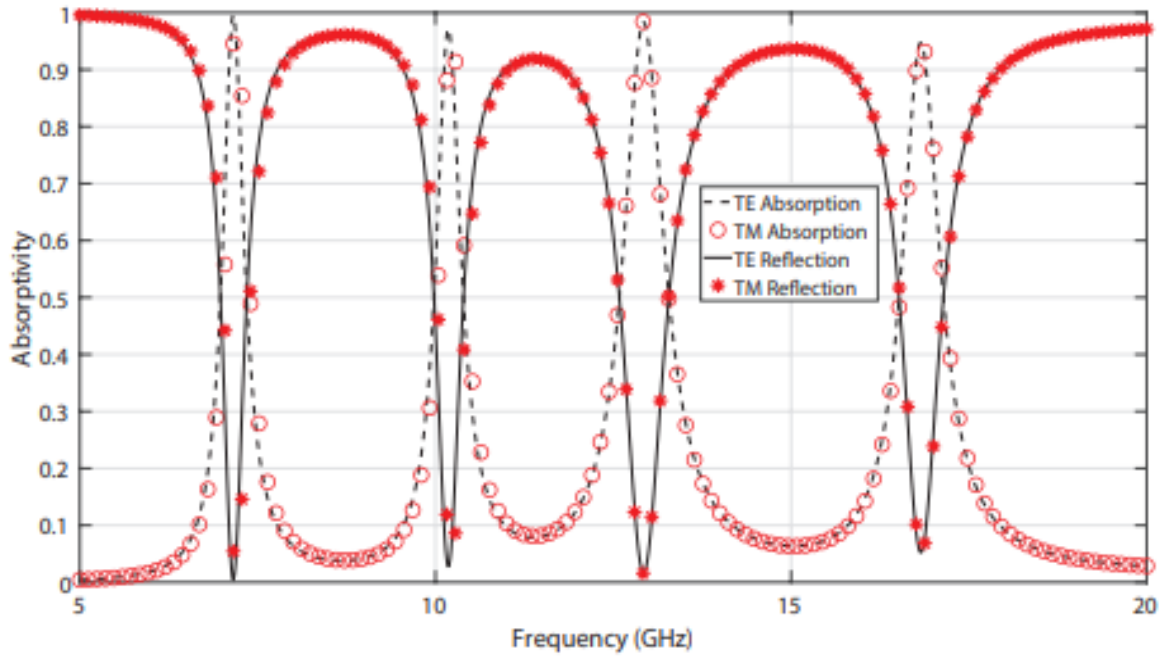
Figure 3.3: Investigation of the absorption characteristics for TE and TM polarized wave
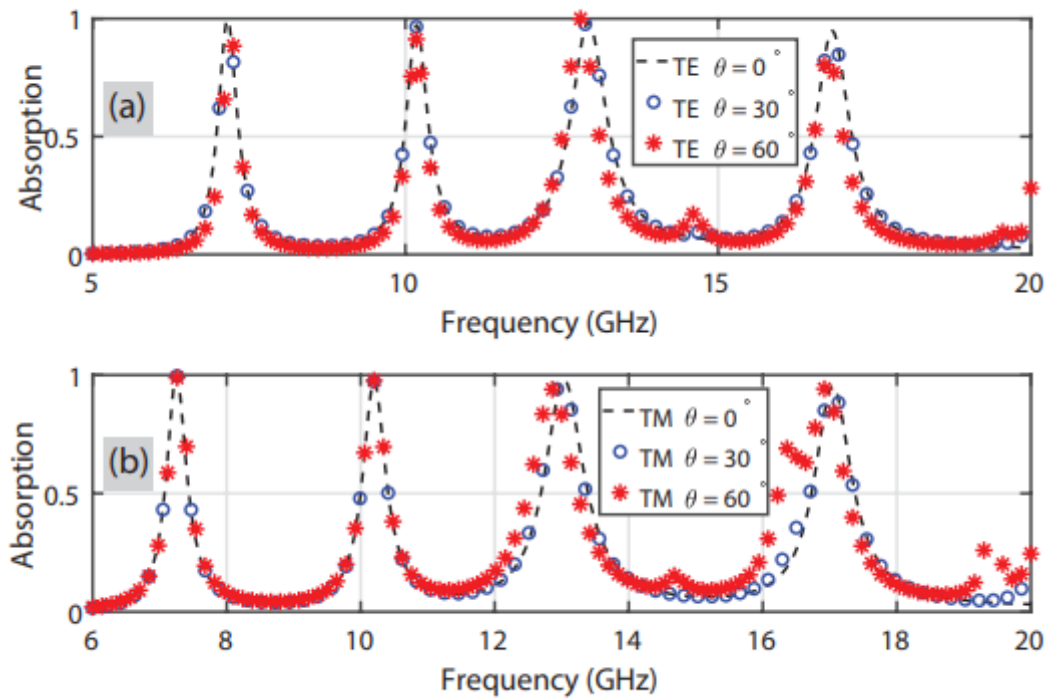
Figure 3.4: Absorption at variation of angles for (a) TE polarized EM waves and (b) TM polarized EM wave
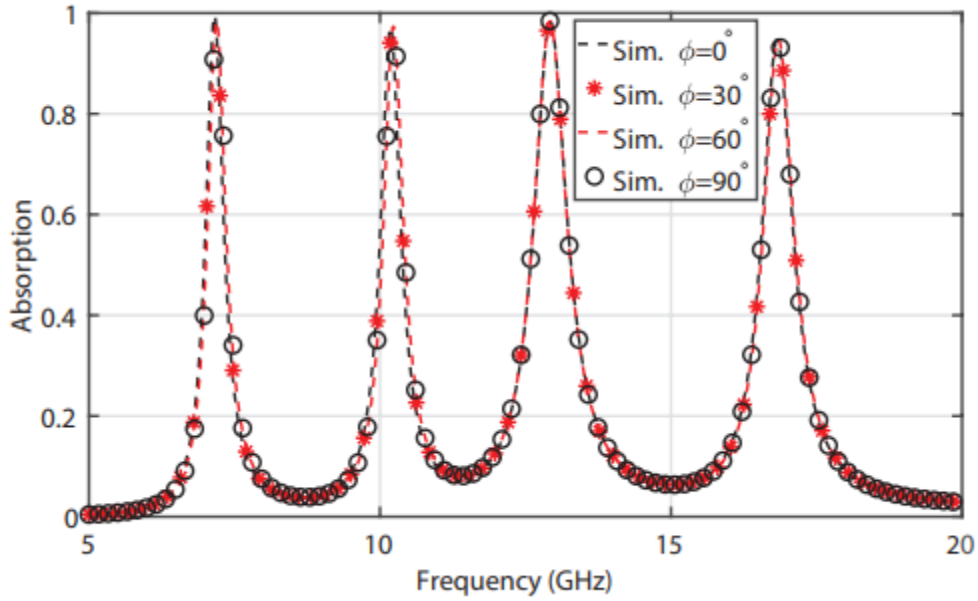
Figure 3.5: Validation of the polarization insensitivity (φ).

3.4   Distribution of Surface Current of designed MA Unit Cell

To get comprehension into the resonance mechanism associated with the incorporated conducting patterns, the current vectors were examined at the four resonance peaks for TE polarized waves, as depicted in Figure 3.6. It is worth noting that for TM polarized waves, the orientation and concentration of the current vectors would be shifted by 90 degrees. Fig. 3.6 (a-d) clearly illustrates that the surface current intensity on the top layer is highly concentrated at the specific conductive patterns corresponding to the respective resonance frequencies. For example, a pronounced concentration of current vectors can be observed at the two circular rings at 7.16 GHz and 10.175 GHz. Similarly, the innermost square structure with a circle inside and the four-gap SRR exhibit significant current concentrations at 16.82 GHz and 12.92 GHz, respectively. Furthermore, it is apparent from Fig. 3.6 that all the incorporated structures exhibit opposite orientations of current vectors when subjected to incoming TE polarized waves. This observation indicates the presence of dipole-like electric resonances within the conducting patterns. The examination of current vectors provides valuable insights into the resonance mechanism and highlights the concentration and orientation of current flow within the relevant conducting patterns.

33

Conversely, when examining the bottom layer, it becomes evident that the current vectors exhibit an opposite direction, as shown in Figure 3.6 (e-h). This observation highlights the interplay of electric, magnetic, and LC resonances within the incorporated patterns of the unit cell, which are responsible for achieving perfect unity absorption at four specific frequencies: f1 = 7.16 GHz, f2 = 10.175 GHz, f3 = 12.92 GHz, and f4 = 16.82 GHz. The designed geometry and orientation of the surface currents in both metal layers effectively prevent the incident electromagnetic wave from penetrating through the uppermost layer at these resonant frequencies. Consequently, the formation of corresponding current loops within the metamaterial structures gives rise to the excitation of magnetic and electric dipoles, ultimately leading to the manifestation of four distinct absorption resonant peaks. The observed opposite direction of current vectors on the bottom layer provides further evidence of the complex interplay between electric, magnetic, and LC resonances within the unit cell. This intricate coupling mechanism facilitates the absorption of electromagnetic energy and enables the formation of distinct resonant peaks.
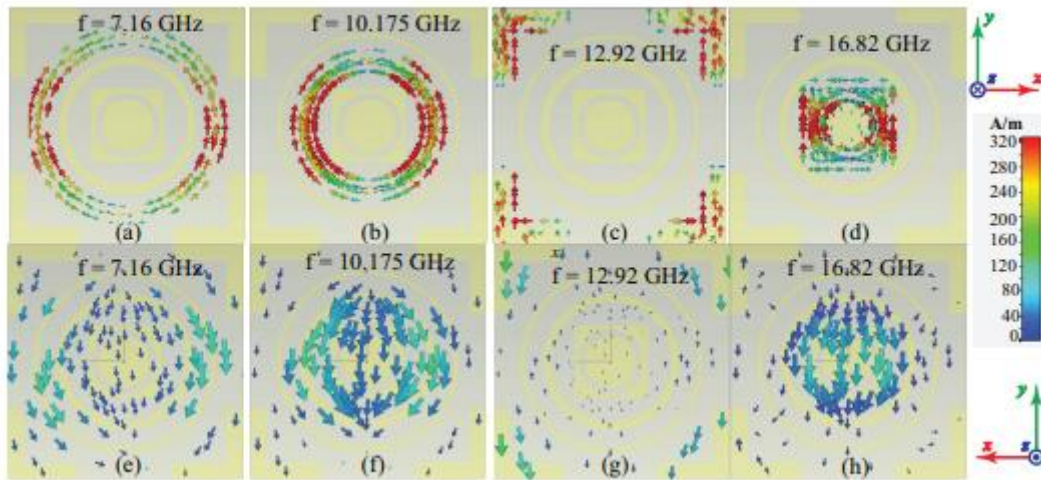
Figure 3.6. Surface Current distribtions at top and bottom layer of MA unit cell.

3.5   Authentication of the meta material nature of the Proposed MA unit cell

To confirm the metamaterial characteristics, the effective permittivity (ε_{reff}) and permeability (μ_{reff}) values were determined by extracting the relevant information from the S-parameters and applying them in the mathematical equations provided below.:

$$\varepsilon_{eff} = 1 + 1/h + \frac{2j\lambda_o}{\pi * h * \sqrt{\varepsilon_o \mu}} \frac{1 - 1/S11}{1 + 1/S11} \qquad (3.4)$$

$$\mu_{eff} = 1 + 1/h + \frac{2j\lambda_o}{\pi * h * \sqrt{\varepsilon_o \mu}} \frac{1 + 1/S11}{1 - 1/S11} \qquad (3.5)$$

Equations (3.3) and (3.4) utilize the substrate thickness represented by h and the free space wavelength denoted by λ_o. By analyzing the S11 values obtained from the CST simulations, the effective permittivity (ε_{reff}) and permeability (μ_{reff}) values were estimated. The resulting values, graphically presented in Fig. 3.7, demonstrate that the effective permittivity and permeability exhibit negative values at most absorption peaks, except for the one at 16.82 GHz. This phenomenon of showcasing unusual dielectric properties in the proposed engineered structure serves as evidence of its metamaterial nature. The corresponding negative numeric values of ε_{reff} and μ_{reff} at the desired frequencies are also listed in **Table 2.**

Furthermore, the metamaterial nature of the proposed design is further validated through the examination of impedance matching theory. Specifically, the S11(ω) values should align with the free space impedance (Z_o) at the corresponding absorption peaks. The numeric values presented in Table 2 display that the real part of the characteristic impedance is approximately equal to the free space impedance. Moreover, the imaginary part is nearly zero at the desired absorption peaks, further reinforcing the metamaterial characteristics of the proposed design.
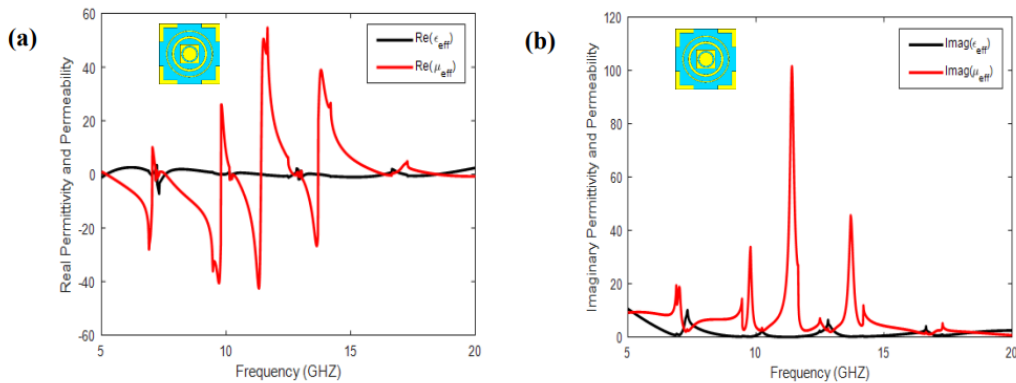
Figure 3.7: (a) Real Permittivity and Permeability (b) Real Permittivity and Permeability.

Table 2: Comparison and values of retrieved parameters w.r.t absorption peaks.

Frequency Peak	Band of Frequency	Re (ε_{eff})	Re (μ_{eff})	Re(znor)	Im(znor)
7.16 GHz	C-band	-2.41	-1.95	0.75	0.02
10.175 GHz	X-band	-1.33	-1.72	1.1	0.004
12.92 GHz	Ku-band	-1.79	-.0.81	0.72	-0.017
16.82 GHz		1.031	0.828	1.09	-0.02

3.6   Analysis of Electric Field Distribution for Absorption Mechanism

Moreover, to gain insights into the absorption mechanism, an examination of the electric field distribution on the proposed metamaterial absorber (MA) was conducted for TE polarized waves at θ = 0˚, as depicted in Fig. 3.8. The findings from Fig. 3.8 (a) reveal that the E-field is identified around the outermost circular ring, corresponding to the absorption peak at 7.16 GHz. This observation indicates the presence of strong surface currents on the outer circular ring and a solid electric field distribution, which are indicative of the permittivity and its association with the electrical resonance. Similarly, at 10.175 GHz, the electric field demonstrates a significant influence along the second circular ring, as depicted in Fig. 3.8 (b). Moreover, the existence of an intense electric field along the lower edges of the four-gap split ring resonator (SRR), as shown in Fig. 3.8 (c), confirms the presence of the third absorption peak at 12.92 GHz. Finally, for the absorption peak at 16.82 GHz, a pronounced electric field can be observed at the innermost square, as depicted in Fig. 3.8 (d). This strong electric field arises from the electric coupling between the innermost square and the inner circular patch.
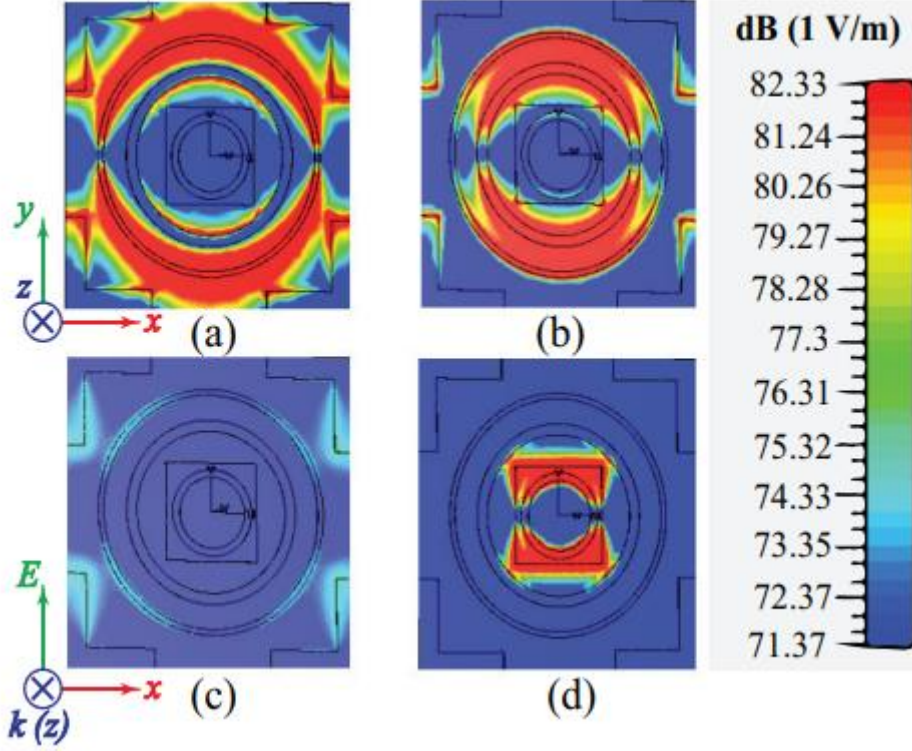
Figure 3.8: Electric Field Distributions of the Proposed MA Unit Cell.

3.7 Experimental Setup and Validation of the Prototype

Subsequently, a prototype of finite size (305 mm × 254 mm), consisting of 30 × 25-unit cells, was fabricated to validate the proposed design. Since a 0.8 mm thick double-sided FR-4 substrate was not commercially available, a double-sided FR-4 was prepared by electroplating copper on both the top and bottom layers of the 0.8 mm FR-4 substrate. The relevant conductive patterns were etched using a laser ablation procedure. Fig. 3.9 (a) showcases a snap of the fabricated prototype, along with a magnified image highlighting the design's shape. To verify the simulation results, the fabricated prototype underwent measurements in an anechoic chamber. The prototype was tested at different values of θ and ϕ to demonstrate the effectiveness of the design.

To facilitate the transmission and reception of EM waves, two identical double-ridged broadband horn antennas with a frequency range of 0.8 GHz to 20.0 GHz were employed. Both antennas were connected to a well-calibrated Anritsu MS46122B vector network analyzer (VNA). To ensure the far-field conditions, a distance of 1.5 m was maintained

between the fabricated prototype and the horn antennas, as illustrated in Fig. 3.9 (b). For TE-polarized EM waves, reflections from the prototype were measured by recording the |S21| values on the VNA. This procedure was repeated for various rotations of θ and ϕ, and the corresponding |S21| values were recorded. The absorption spectra were obtained using the expression A = 1 - |S21|. Fig. 3.10 presents the absorption spectra, providing a detailed analysis of the absorptivity. Additionally, Fig. 3.9 (b) showcases a photograph of the measurement setup. The comparison of results displayed in Fig. 3.10 (a-c) reveals that the experimental findings align with the simulated results for different values of θ (0°, 30°, 60°) for both transvers electric and transverse magnetic polarized EM waves. The absorption factor remains above 90% at the four distinct peaks and remains consistent even for oblique angles of incidence. However, a slight discrepancy in the absorption peaks between the experimental and simulated results can be credited to the lossy characteristic nature of the FR-4 substrate at higher frequencies. Additionally, the occurrence of additional harmonic peaks may contribute to the observed spatial dispersion phenomenon at varying incident angles θ. Nevertheless, due to the subwavelength structures and utilization of multiple resonant elements within a unit cell, the original absorption peaks at the desired frequencies are minimally affected by changes in θ, indicating the angular stability of the proposed design. The polarization-insensitive analysis of the proposed design, achieved by varying the Phi angle (ϕ) from 0° to 90°, is represented in Fig. 3.10 (d). Overall, a good concurrence can be observed among the simulated and measured results. The absorption characteristics of the structure at the four distinct peaks remain unchanged with variations in the polarization angle. Consequently, it can be concluded that the proposed design exhibits polarization insensitivity. Furthermore, a comprehensive comparative analysis between the proposed metamaterial (MA) and existing MA designs from the literature is performed and organized in Table 3.
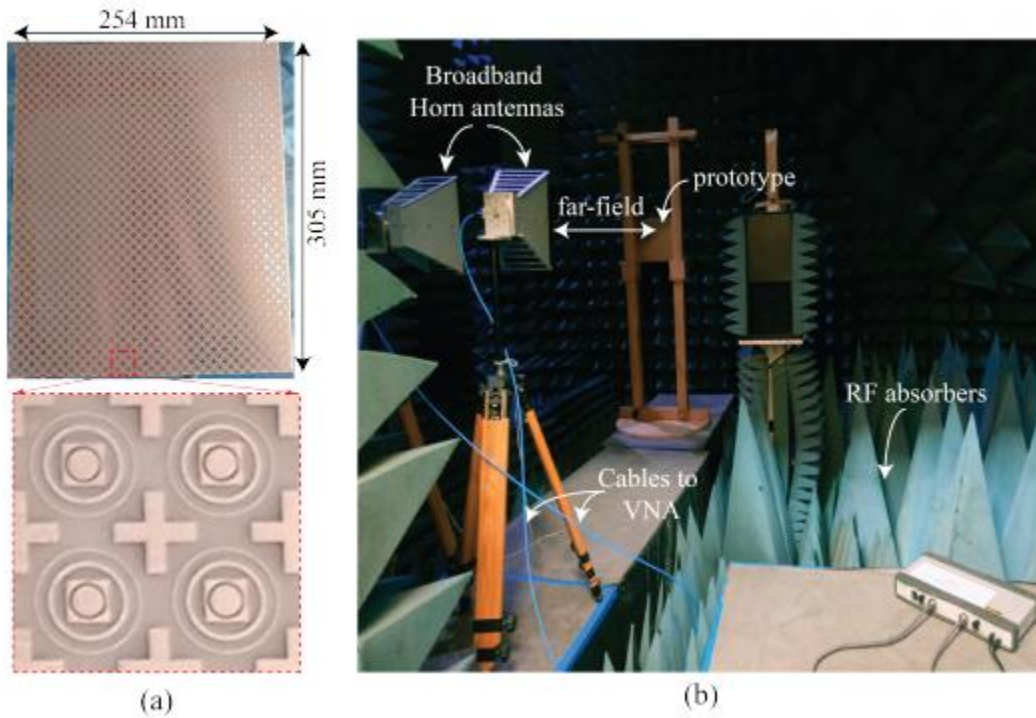
Figure 3.9: (**a**) Fabricated Prototype of MA (**b**)Experimental environment for measurement.
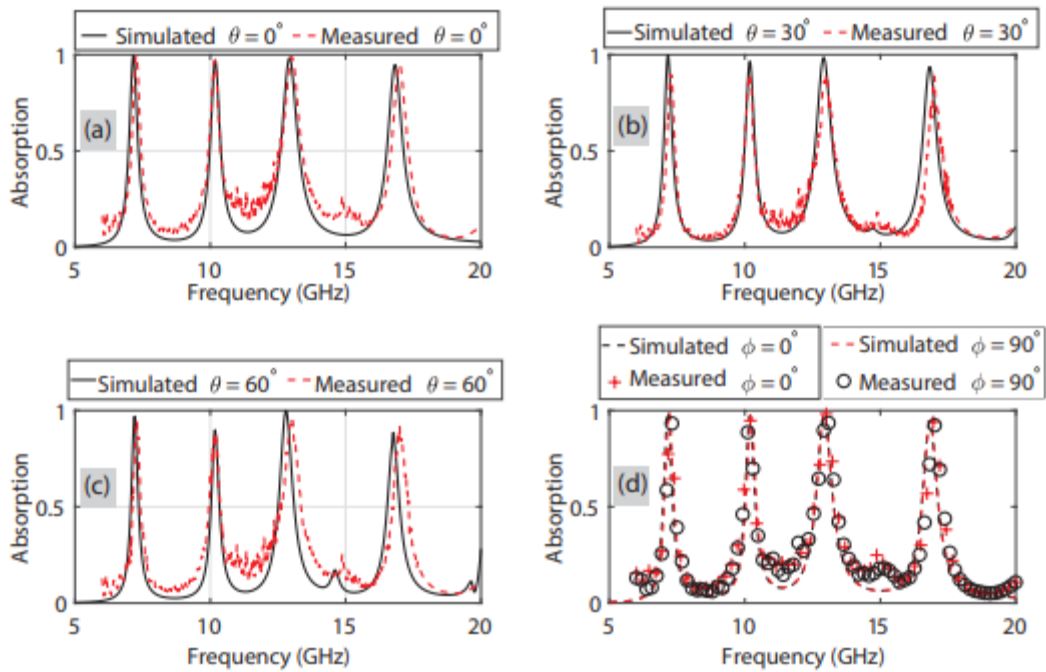
Figure 3.10: Experimented and simulated absorptivity comparison (a) For EM wave at TE Mode at $\theta = 0°, 30° \ and \ 60°$. (b) Different values of φ for 0˚and 90˚

Table 3: Comparative Analysis of Proposed Metamaterial Absorber with Recent Relevant Studies.

Design/ Reference	Absorption Peaks (GHz)	Insensitivity to Polarization (φ)	Oblique Angle Stability (θ)	Substrate Thickness	Observations
[105]	12.79- 16.64 GHz	till 70˚	As θ increases absorption decrease	1.00 mm	• Sensitive to φ • Less angular stability •
[106]	4.52-25.42 GHz	Not reported	Up to 45˚	5.0 mm	• Less angular stability • Not flexible
[107]	5.49-16.84 GHz	As θ increases absorption decrease	As θ increases absorption decrease	4.0 mm	• Less angular stability • Lesser polarization-insensitive • Larger unit cell dimensions
[109]	7.8-14.7 GHz	Not reported	Up to 40˚	5.0 mm	• Thick design
[110]	Absorption reduces to MHz Upon variation in size	Up to 45˚	Up to 30˚	0.60 mm	• Angular stability is less. • Less absorptivity
[111]	7.64-10.4 GHz	till 30˚	till 30˚	1.60 mm	• Angular stability is less. • Polarization-sensitive
[112]	7-12.8 GHz	till 70˚	till 45˚	3.4 mm	• Angularly unstable • Thick substrate
[113]	2.3-18.9 GHz	till 45˚	till 45˚	11.30 mm	• Angularly unstable • Thick substrate
[114]	5.69-15.12 GHz	till 0˚	till 45˚	4.4 mm	• Angularly unstable • Polarization-sensitive
[115]	8.37-20.1 GHz	Up to 90˚	Up to 45˚	3.65 mm	• Less angular stability • Thick substrate
[116]	5.12 - 5.59 GHz	Not reported	Up to 45˚	6.76 mm	• Less

					Polarization-Insensitive • Thick substrate
[117]	4.7-50 GHz	Not reported	Up to 40°	6.5 mm	• Polarization-sensitive • Thick substrate
Proposed Work	7.16, 10.175, 12.92 and 16.82 GHz	Up to 90°	Up to 60°	0.8 mm	• Excellent absorptivity • Good Polarization-Insensitivity • Decent angular stability • peaks • Thin design

3.8   Discussions

We have successfully developed, simulated, and fabricated a single-layered metamaterial absorber (MA) that exhibits remarkable performance in terms of efficiency, profile, and absorption across multiple frequency bands. Our proposed MA demonstrates exceptional absorption capabilities, having absorption of more than 99% at the desirable resonant frequency peaks of 7.16, 10.175, 12.92, and 16.82 GHz when subjected to normally incident electromagnetic waves. Moreover, the designed MA has shown angular stability at higher angles as well i.e., up-to 60 degrees and along with the polarization insensitivity up to 90 degrees. This characteristic is attributed to the symmetrical C4 structure employed in our design. The designed MA has also been evaluated thoroughly by discussing and analyzing its surface current distribution as well as electric field distribution. To further validate our design, a prototype consisting of 30 × 25-unit cells was fabricated and tested. The experimental results closely matched the simulated outcomes, confirming the accuracy and reliability of our design approach. With its impressive absorption characteristics, our proposed MA holds great potential for applications in electromagnetic shielding and reduction of radar cross-section (RCS). applications.

Chapter 4

Ultra-thin, Wideband Modified Square Shaped with Chip resistors Metamaterial Absorber for RCS reduction applications.

Introduction

This chapter comprises of the development, designing and characterization of wideband metasurface absorber in planar and as well as in conformal or cylindrically bent geometrical surface. The design has shown outstanding polarization insensitivity as well as angular stability at different angles. The Cyclic-4 (C-4) symmetrical design comprises of modified metallic (copper) square-shaped structures stacked with 04 x lumped resistors whose optimization has been numerically achieved using CST microwave studio. Under the incidence of EM wave, the designed metamaterial absorber has achieved reflection coefficient reduction smaller than -10 dB for fractional bandwidth (104.14%) and having the thickness of $0.097\lambda_L$ (where λ_L represents the starting operating frequency of metamaterial absorber). Proposed broadband metamaterial absorber having ultra-thin substrate thickness with only 0.15mm and having polarization insensitivity $\phi = 90$ ° with absorption up-to 99.9% and for subsequently varying angles in TE and TM modes the absorption is greater than 90% till 45˚ ranging from 7.30 to 23.16 GHz. The designed broad band absorber has perfect RCS reductions and EM shielding capabilities.

To validate the principles of designed metamaterial absorber and its simulated results, upon successful fabrication of the metamaterial absorber prototype has been undertake, a thorough examination revealed a remarkable agreement between the observed experimental results and the simulated outcomes. Moreover, to authenticate the radar stealth application the same design has been simulated for different geometrical surfaces which includes planar and conformal both.

The chapter is divided into various sections. Section **4.1** comprises structural designing and layout and describing designing methodology of unit cell. While section **4.2** comprises of absorption characteristics at different oblique and polarization angles. Section **4.3** tells us about the absorption mechanism of proposed MA, whereas **4.4** describes Surface current distribution and sub-section **4.5** comprises of equivalent circuit model. Section **4.6** describes analysis of RCS reduction of the proposed metamaterial absorber, Section **4.7** comprises of Fabrication of Designed MA for Experimental Results and concluding remarks are presented in Section **4.8**.

4.1   Structure Designing and layout of Proposed MA Unit Cell

4.1.1   Designing Methodology of a Unit Cell

To achieve broadband absorbance with wide angular stability and polarization insensitivity, the design of meta-surface absorbers often involves utilizing symmetrical geometries. Square-shaped ring structures have been used due to their polarization insensitivity and inherent symmetry. To avoid weak resonances and achieve a broad absorption bandwidth, the electrical length of the square rings has been kept at one wavelength long, Encompassing a broad spectrum of frequencies 7.3 to 23.16 GHz. Therefore, the designed MA consists of modified square-shaped metallic patch and one inner square shaped ring as well printed on the dielectric substrate and is grounded by an air spacer used for zero transmission whose pictorial view is depicted in Fig.4(a). The substrate which has been used as a dielectric spacer is FR-4 (having ϵ_r=4.3 and loss tangent δ=0.025) with thickness of only 0.15mm. Similarly, the thickness for the air spacer has been kept to 4mm. The top metallic modified square shaped structure and the ground is made of thin copper film (having conductivity σ =5.8 x 10^7 S/m and thickness of 0.02mm). Overall augmented dimensions of the proposed design are displayed in Fig.4(b). To increase the absorptivity response of the proposed broadband metamaterial design 04 x chip resistors with value R = 200Ω were reinforced on each unit cell. The resonance frequency of a squared ring metasurface absorber can be estimated mathematically using the following equation:

$$f = \frac{c}{2*L_1+L_2}$$

(4.1)
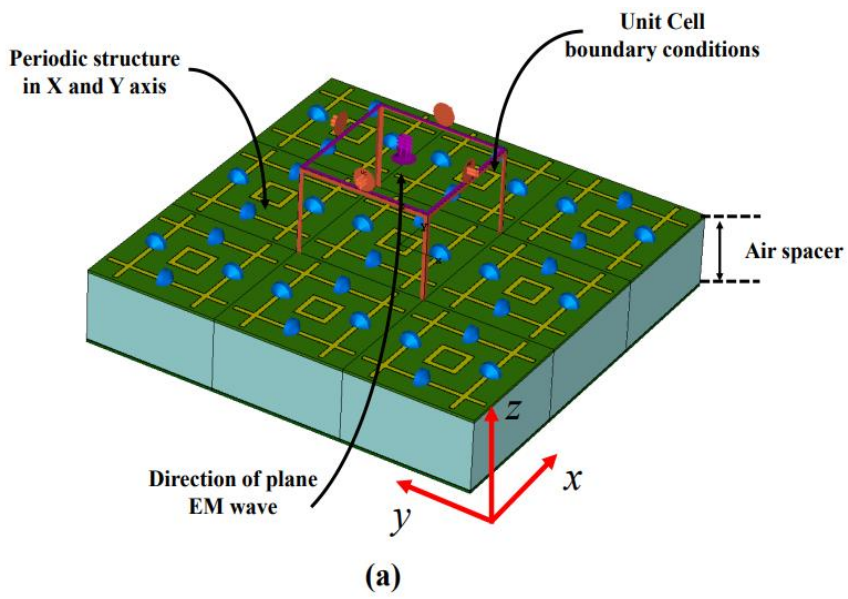
Fig.4.1 (a) Proposed 3D MA Design.

(b)
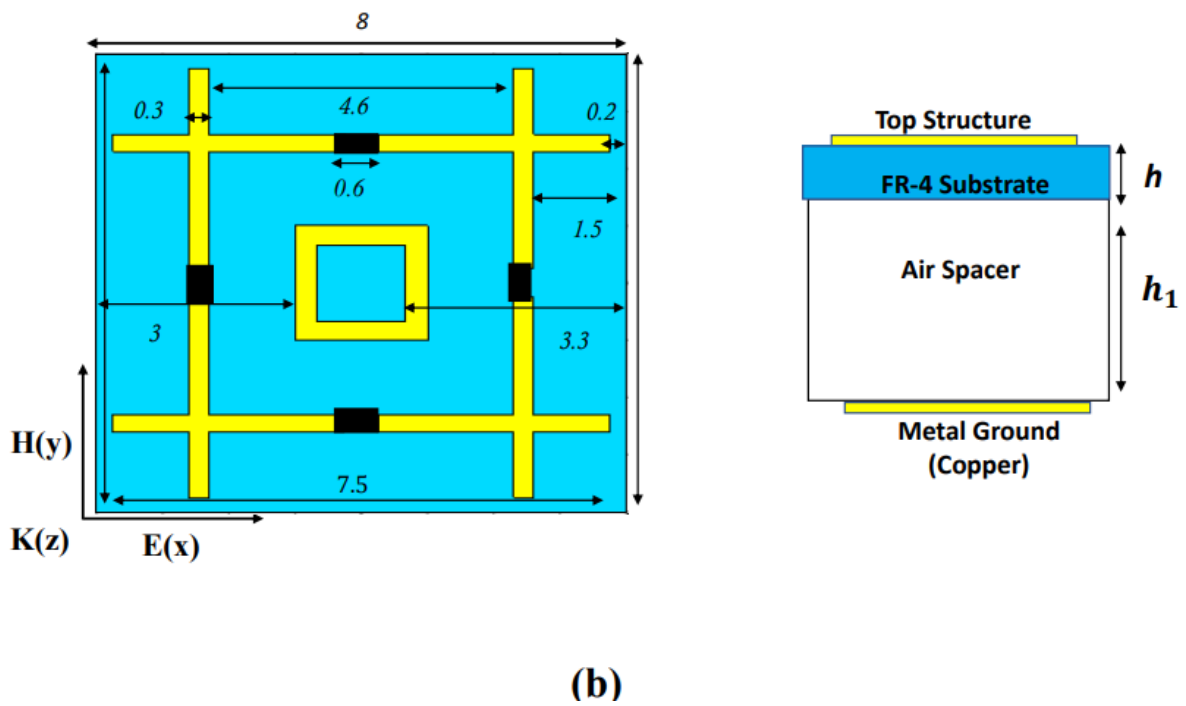
Fig.4.1 (b) Complete layout of the proposed MA

4.1.2 Designing of a Unit Cell without lumped Resistors.

The proposed MA unit cell was tested with and without SMT resistors, while testing it without chip resistors the designed MA unit has exhibit very less absorption which shows that the adding of resistors though increases the ohmic losses but eventually helps in attaining the broad band frequency absorption band. Same is demonstrated in Fig. 4.2 (a-b).
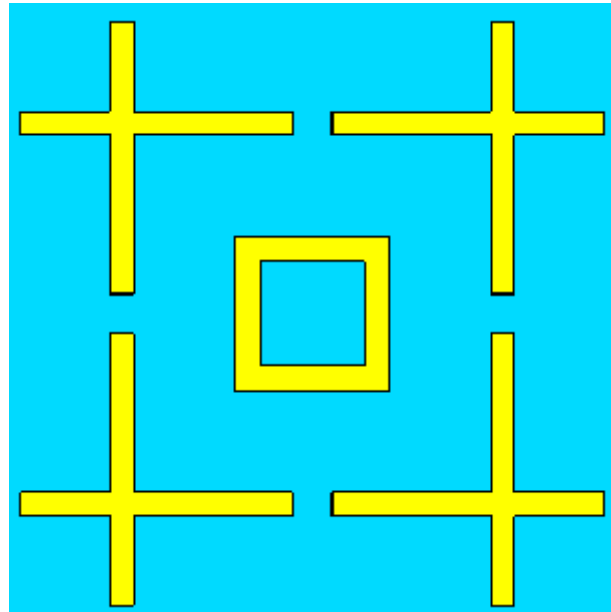
Fig.4.2 (a) Layout of Proposed MA Unit Cell without chip resistors
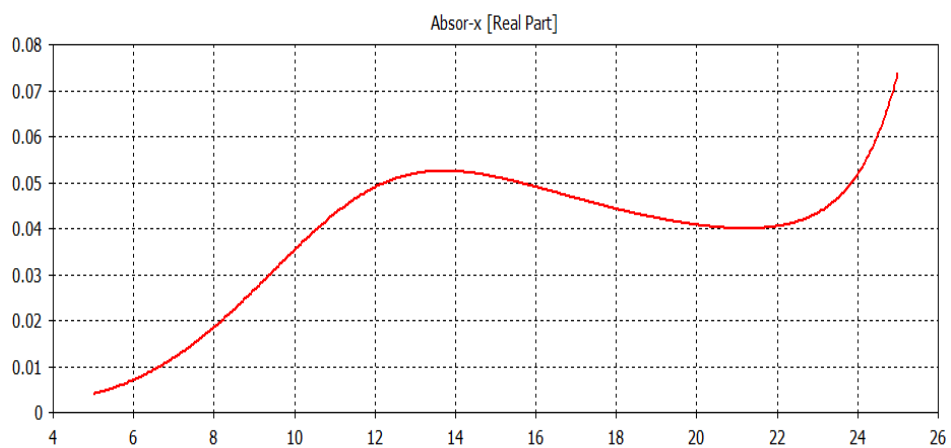
Fig.4.2 (b) Absorptivity vs Frequency graph for without resistors

4.1.3 Designing of a Unit Cell with varying values of lumped Resistors.

In this case the designed MA unit cell is tested for different ohmic values ranging from 50 to 300 ohms same is displayed in Fig. 4.3, where it is clearly visible that the best and much greater broad band absorption has been achieved at 200 ohms ranging from 7.30 to 23.16 GHz.
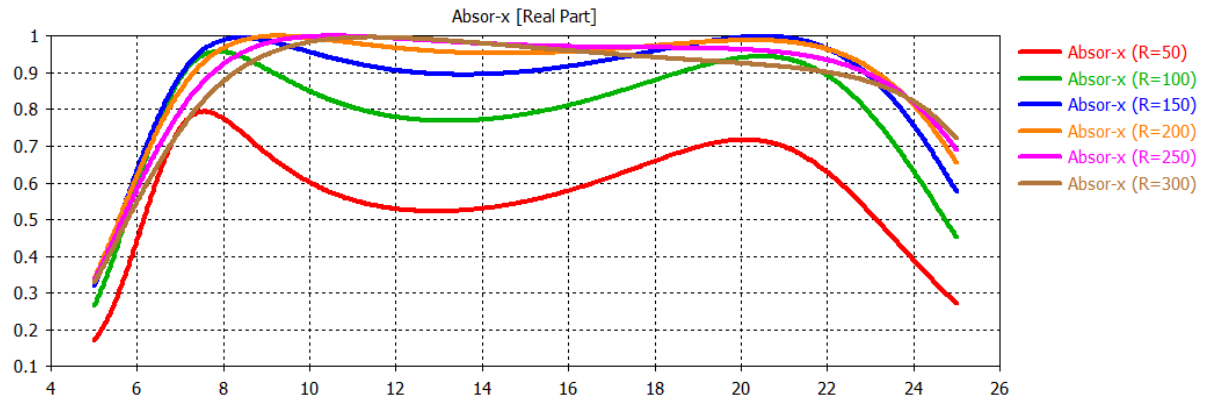
Fig.4.3 Absorptivity vs Frequency graph with different resistors values.

4.2 Physics of Absorption of the Proposed MA Unit Cell

To determine the absorptivity factor or absorption coefficient of the proposed metamaterial absorber under the incidence of normal EM wave, A(ω) is given by:

$$A(\omega) = 1 - |S11(\omega)|^2 - |S21(\omega)|^2 \qquad (4.2)$$

To achieve the ideal metamaterial absorber, it is crucial to maximize its absorption coefficient by minimizing both the reflection coefficient (S_11) and transmission coefficient (S_21). This objective can be realized by cautiously optimizing the geometric dimensions of the unit cell to ensure impedance matching between the absorber (Z(ω)) and free space (Z_O), where Z(ω) = Z_O. By precisely tailoring the unit cell's geometrical parameters, the reflection coefficient can be effectively suppressed, approaching zero. Consequently, when employing a copper metallic ground, the transmissivity coefficient (S_{21}) is reduced to zero, resulting in an enhanced absorption coefficient (A(ω)) given as:

$$A(\omega) = 1 - |S11(\omega)|^2 \qquad (4.3)$$

Moreover, under the incidence of normal EM wave the value of reflection coefficient $S_{11}(\omega)$ remains less than -10 dB from 7.30 to 23.16 GHz with the maximum dip of -38.18 dB at 9.26 GHz which subsequently corresponds to 99.99% absorption.

To assess the reliability and suitability of the developed meta surface absorber as a benchmark device, an analysis was conducted to examine its absorption capabilities when subjected to variations in both incidence and polarization angles.

4.2.1 Angle of incidence variation

The proposed metamaterial absorber was thoroughly deliberated and tested under different oblique incident angles. Under the TE-polarized EM-wave and by varying incidence angle from 0 to 45 degrees and the absorptivity remains ≥ 90%. For the TM-polarized EM wave by varying the angle the absorptivity remains ≥ 90% till 45 degrees in the given regime of frequency i.e., (7.3-23.16 GHz) with minute reduction or slight right shift in the frequency resonant band as depicted in Fig.4.4(a-b).

(a)
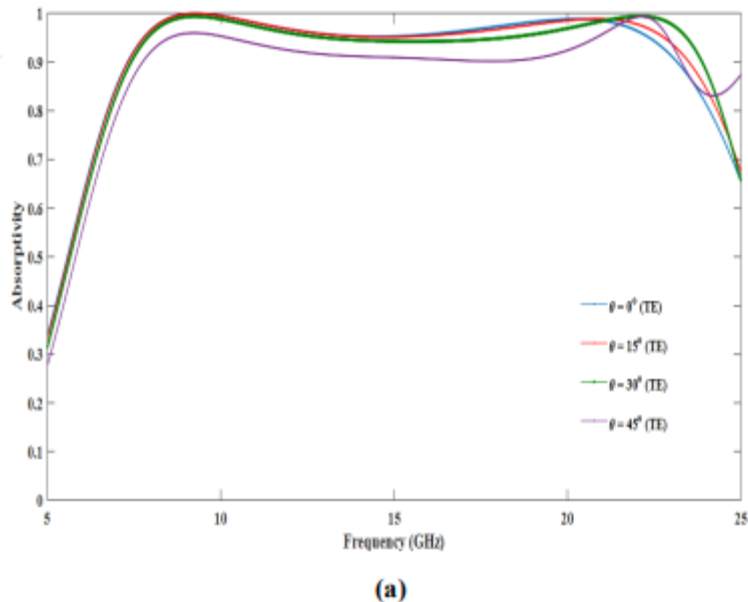
Fig.4.4 (a) Absorption of proposed MA at variation of angles along TE Mode.
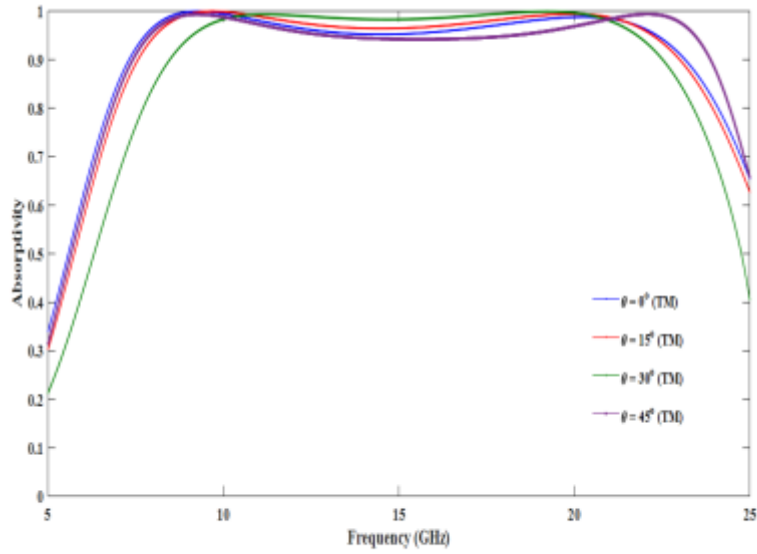
(b)

Fig.4.4 (b) Absorption of proposed MA at variation of angles along TM Mode.

4.2.2 Polarization angle variation

Since the designed metamaterial absorber is having four-fold Cyclic-4 (C-4) rotational symmetry and its response to all polarization angles have been also thoroughly analyzed and it has been observed that the suggested design remains insensitive to polarization till $\phi=90°$ same is displayed in Fig.4.4 (c).
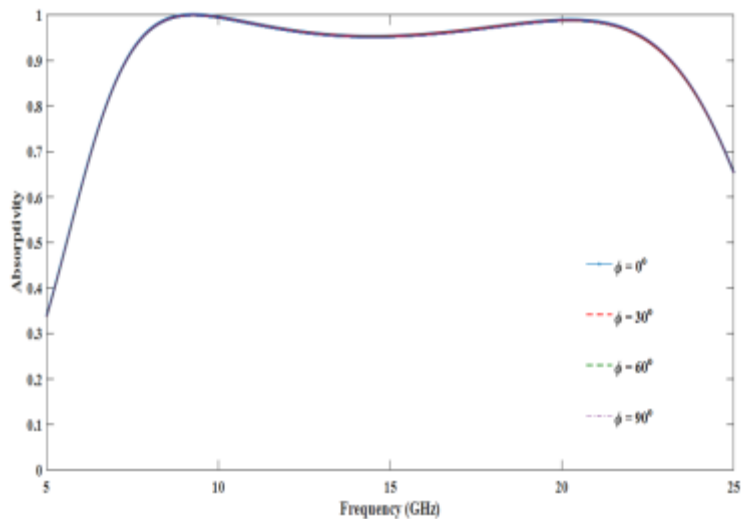
(c)

Fig.4.4(c) Absorption Spectra of proposed MA at different (φ)

4.3   Absorption Phenomena of Proposed MA Unit Cell.

To gain insights into the absorption mechanism exhibited by the metamaterial absorber design, an in-depth analysis of the power loss density distribution was conducted at the extreme operating frequencies, i.e., 7.3 and 23.16 GHz. The findings obtained from the examination, as illustrated in Figure 4.5(a-b)that for TE-polarized EM wave incidence the magnitude of the maximum power dissipation density is maximum along the chip resistors which are mounted along the vertical length of modified square shaped metallic structure and while for TM-polarized EM wave incidence the magnitude of the power loss density is maximum along the chip resistors mounted along the horizontal length of modified square shaped metallic structure a displayed in fig. 4.5 (c-d). From the figures is clearly visible that the majority of energy losses are because of the resistors who are responsible for the ohmic losses which are attached along the vertical and horizontal lengths of the modified square shaped structure. It is pertinent to mention that here absorption of EM wave in designed MA is due to different losses in the metallic patch or structure which includes ohmic, conduction and dielectric losses. Here the vital role for the broadband absorption is played by the lumped resistors present in the design. Moreover, a strong electric field concentration has been found around the specific parts of designed MA which results in an absorption band depending upon the electric length of the modified square shaped structure.
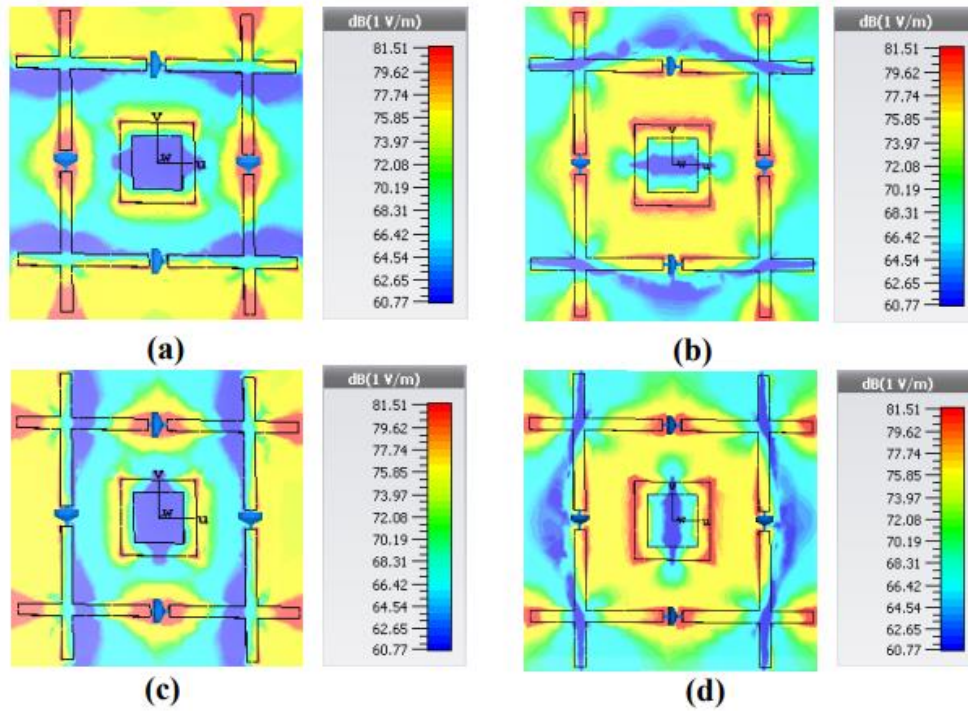
Fig.4.5 Electric Fields distributions at (a) 7.3 and 23.16 GHz for TE polarized EM wave (b) 7.3 and 23.16 GHz for TM polarized EM wave.

4.4   Examination of Surface Current distribution at desired frequencies

The distribution of surface current was analyzed at lowest and highest frequencies of the broadband MA i.e., (7.30 and 23.16 GHz) and it has been observed that the surface current at the top metallic layer and the ground are in anti-parallel direction at 7.3 GHz around the conducting electrical lengths of metallic structure which gives negative permeability and ultimately results in magnetic dipole effect at the desired resonant frequency. Consequently, for 23.16 GHz resonant frequency the direction of surface current on the top metallic layer and ground are parallel to each other around the conducting electrical lengths of metallic structure thus forms negative permittivity in TE and TM modes respectively. Same is illustrated in Fig.4.6(a-d).
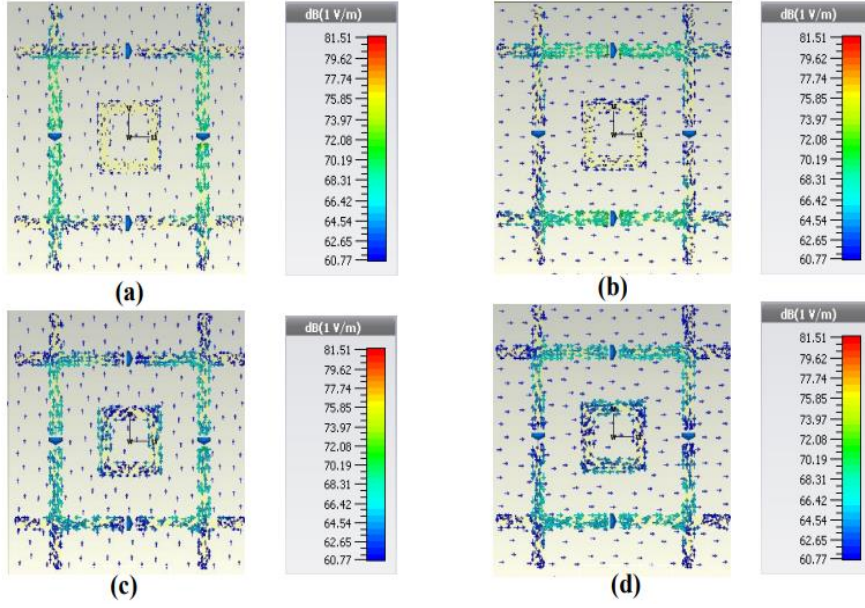
Fig.4.6 Surface Current distributions at 7.30 and 23.16 GHz.

4.5   Designing of Equivalent Circuit Model (ECM).

The equivalent circuit model of the proposed meta material is shown in Figure 4.7(a). The top layer having the whole metallic patch (structure) is loaded with 04 x chip resistors which are represented through RLC series circuit connected in parallel as depicted in figure. The metallic patch is represented as the inductor and due to the path of current on the metallic patch inductance is created and the gap between the two metallic elements is represented through capacitor or capacitance respectively. Here, the equivalent losses within the metallic patch are represented as R, L and C, where i=1 is for resistive line in vertical direction and i=2 is for the resistive line in horizontal direction and i= 3 is for the inner square of the proposed design.

$$Z_{MA} = (R_1 + j\omega L_1)||(R_2 + j\omega L_2)|| \left(j\omega L_3 + \frac{1}{j\omega C_3}\right) \tag{4.4}$$

The air spacer and dielectric substrate (FR-4 lossy) are counted as the transmission lines having the lengths represented as t_a and t_g and the overall impedance Z_1 seen from the air spacer is given as:

$$Z_1 = j\left(\frac{Z_o}{\sqrt{\epsilon_{r_1}}}\right) tan\beta_1 t_g \tag{4.5}$$

51

where Z_o represents the characteristics impedance of free space, β is the phase constant, ϵ_{r_1} is the dielectric constant while t_g is the thickness of air spacer with copper ground. The FR-4 substrate, characterized by its lossy properties, can be effectively modeled as a transmission line with a defined length denoted as t_s, allowing the input impedance to be expressed as:

$$Z_2 = j\left(\frac{Z_o}{\sqrt{\epsilon_{r2}}}\right) \frac{Z_1 + j\left(\frac{Z_o}{\sqrt{\epsilon_{r1}}}\right) tan\beta_2 t_s}{\frac{Z_o}{\sqrt{\epsilon_{r1}}} + jZ_1 tan\beta_2 t_s} \tag{4.6}$$

here, t_s and β are the phase constant where $\beta = \frac{\omega\sqrt{\epsilon_r}}{c}$. Therefore, the input impedance of the proposed metamaterial is given as

$$Z_{in} = Z_{MA}||Z_2 = \frac{Z_{MA}Z_2}{Z_{MA}+Z_2} \tag{4.7}$$

The parallel circuit discussed earlier exhibits resonance when the admittance (Y_{MA}) of the top metallic structured layer matches the magnitude but differs in sign from the admittance (Y_s) of the layer of substrate. This condition leads to a purely real input impedance value, indicating the optimal state for resonance. To design and simulate the circuit, the Keysight ADS software was utilized, allowing for precise optimization of the circuit parameters. The optimized values and corresponding results are presented in Figure 4.7 (b), providing a visual representation of the achieved resonance and its associated characteristics.

(a)   (b)
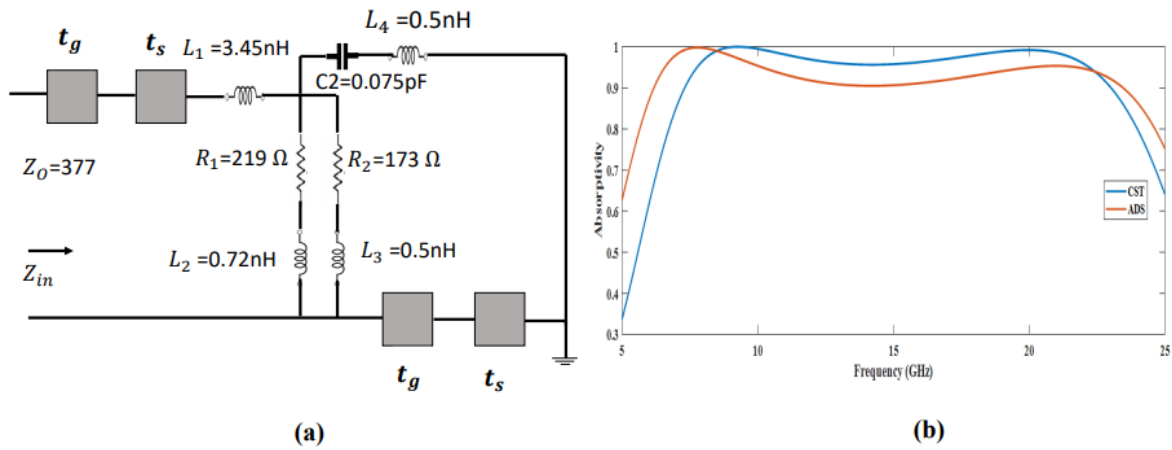
Fig.4.7(a) ECM MA unit Cell (b) Simulated results on CST microwave studio versus ADS.

52

4.6. Analysis of RCS reduction of designed MA

Major advantages of radar stealth applications are to keep the Radar Cross-Section or RCS of objects, especially like military aircraft or ships small to keep them invisible or make enemy radar's unable to detect them. There are many ways to keep RCS of these targets small by size, shape, aspect, or material (MASS), conformal structures are the key contributors towards the RCS of targets. Hence, it is worth mentioning to discuss the effect of RCS reduction on metasurfaces. The RCS of the MA was calculated by applying far-field conditions on the design on CST microwave software, moreover for the measurement of RCS the RCS of Perfect Electric Conductor (PEC) was also measured along with the designed MA for comparison which has been illustrated and explained in chapter as well. Target RCS (σ) is stated as:

$$\sigma = 4\pi \lim_{R \to \infty} R^2 \frac{E_S^2}{E_i^2} \tag{4.8}$$

In the context of radar detection, the distance between the detection radar and the target is denoted by "R." The intensity of E-field wave that has scattered from the target is represented as "E_s," while the E-field intensity is denoted as "E_i." of the incident wave. These parameters play a crucial role in assessing the interaction between the radar waves and the target, allowing for the analysis of signal strength and the extraction of valuable information regarding the target's characteristics.

4.6.1 Absorption mechanism of Proposed Metamaterial for Planar Surface

To understand capabilities of RCS reduction of proposed MA design a 11 x 11-unit cells of the same structure was designed to analyze its capabilities against the monostatic as well as bistatic radar systems. For the comparison a PEC plate having the same size as that of MA was designed and simulated. Under the broad frequency spectrum RCS reduction for monostatic radar system (where transmitter and receiver are located at same place) for both planar PEC as well as MA are calculated. Figure 4.8(a-d) presents the monostatic radar cross-section (RCS) patterns under normal incidence of electromagnetic waves for the planar metamaterial absorber (MA) (depicted in black), as well as the planar perfect electric conductor (PEC) (depicted in red). Additionally, the far-field patterns at the lowest, central, and highest frequencies of 7.3 GHz, 15.2 GHz, and 23.16 GHz are displayed. The figure clearly demonstrates that the proposed MA achieves a significant reduction in RCS, reaching

nearly -20 dB across the given frequency range of 7.3 - 23.16 GHz. Furthermore, the designed MA exhibits substantial RCS reduction at the specified frequencies.
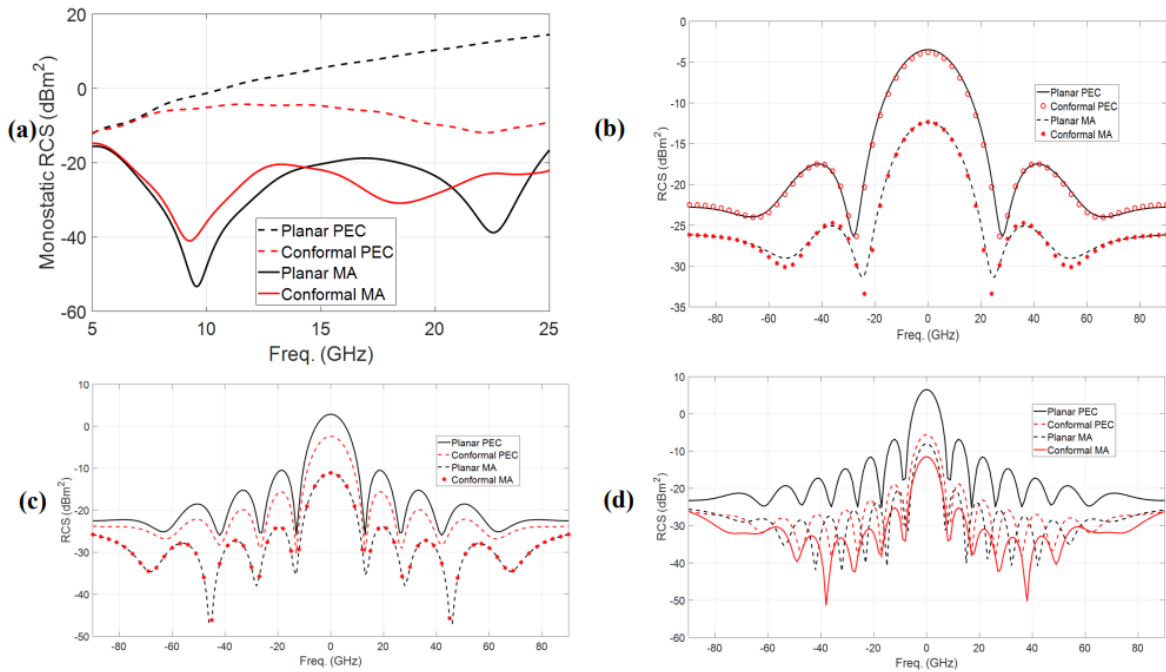
Fig4.8. (a) Monostatic RCS pattern for planar and bent MA and PEC (b) Pattern of Far-field at 7.3 GHz (c) 15. 4 GHz (d) 23.16 GHz

4.6.2 Exploring the Absorption Mechanism of Metamaterials on Curved Surfaces

The proposed metasurface absorber in this case comprises of 11 x 11-unit cells cylindrically bent at a radius of curvature r=100mm to evaluate and understand its RCS reduction characteristics. As a reference the cylindrical bent PEC of the same size and radius of curvature was designed to calculate the RCS for comparison with the proposed cylindrically bent MA. The three-dimensional representation of a cylindrically bent Perfect Electric Conductor (PEC) and the proposed Metamaterial Absorber (MA) can be observed in Figure 4.9(a-b). Figure 4.8(a-d) illustrates the radar cross-section (RCS) of the cylindrically bent perfect electric conductor (PEC) and the proposed metamaterial absorber (MA) when subjected to normal incidence of an electromagnetic wave.
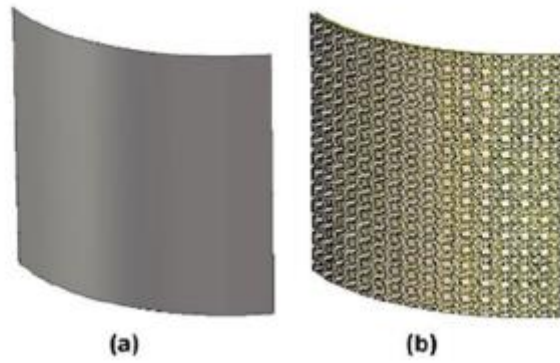
Fig4.9. A three-dimensional visualization of a cylindrically bent Perfect Electric Conductor (PEC) and the proposed Metamaterial Absorber (MA)

4.7.   Fabrication of Designed MA for Experimental Results

For authentication of the simulated results the prototype of designed MA was constructed, having the size of 12 x 10 inches (30 x 25-unit cells) using smart PCB technology. The design was etched using copper metal used to form metallic patch on the top layer of only 0.15mm thick FR-4 substrate. Once the fabrication of metallic designed MA on FR-4 substrate was done, chip resistors (3000 in numbers) were soldered on the metallic design having value of 200Ω using technology known as surface mounting and padding. Afterwards, Teflon strips were used to separate the top dielectric layer (substrate layer) from the ground metallic layer having air spacing of 4mm **Fig**.4.10(a-b) exhibits top metallic layer, and the whole testing and experimental setup.

For the experimental setup was equipped with 02 x horn shaped antennas manufactured by A-INFOMW having frequency ranges from 0.8 to 25 GHz one used as transmitter and the other one for receiving the EM waves., the vector network analyzer (VNA) MS46122B. was used for the measuring of received antenna signals connected to horn antennas. Before the measurement the conditions were satisfied and VNA was calibrated (by placing metallic plate having the same size as that of prototype in the far-field region) to include the transmission losses and tolerance errors for the calculations of reflection reduction. The prototype MA was placed at 1.3m from the horn shaped antennas fulfilling the far field obligations. Upon incident of the normal EM wave the experimental results were found making good settlement with the simulated results. Slight shifting of resonant peak (broadband peak at different

angles) is due to the mutual coupling between the resonating elements, lossy nature of FR-4 material and the losses during the measurements as shown in Fig.4.11 (a-d). Similarly, the experimental setup for the cylindrically bent proposed MA along with its fabricated results are in Fig.4.12 (a-b).
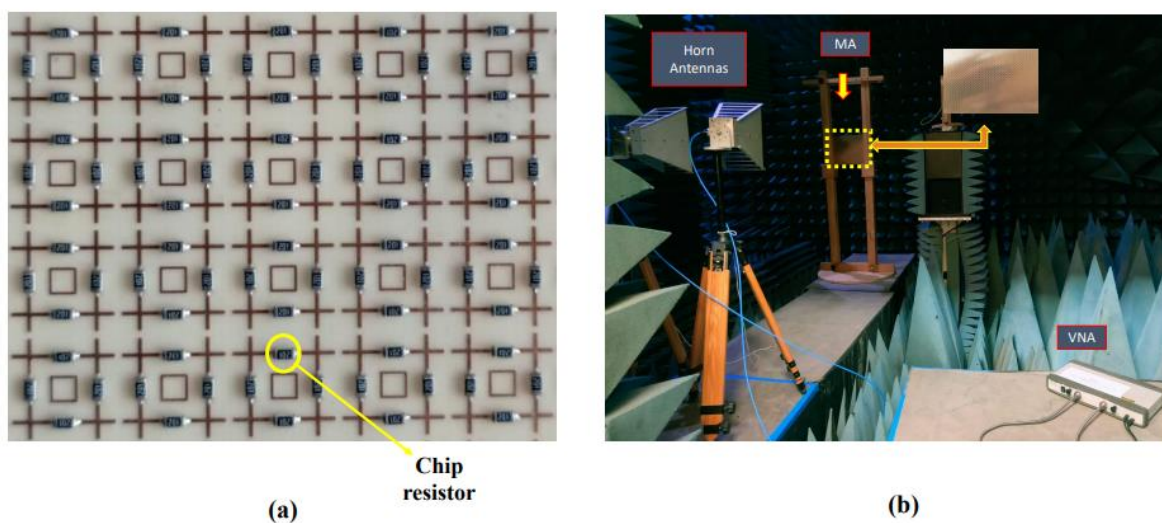
Fig.4.10 (a) Fabricated Prototype (b) Experimental Setup
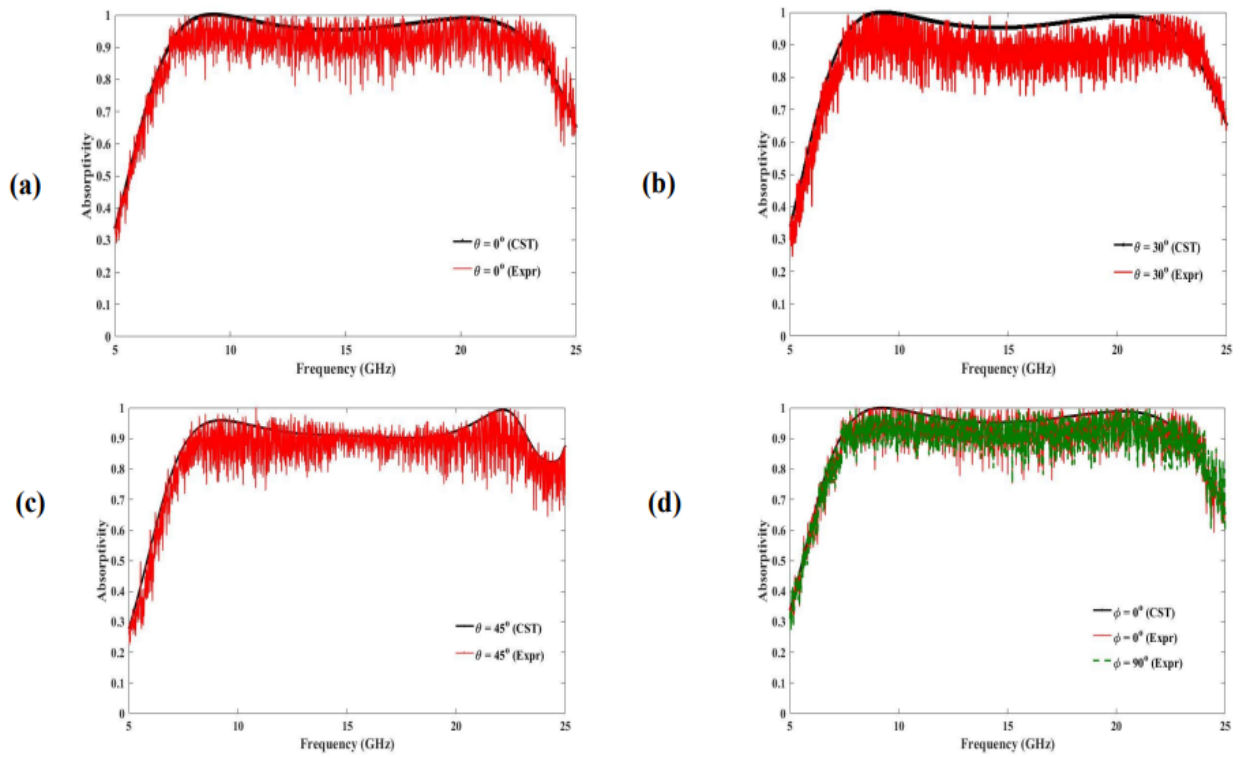
Fig.4.11 Experimental results at different angles (θ)
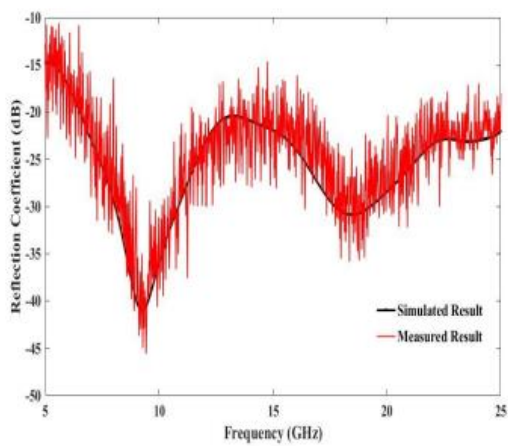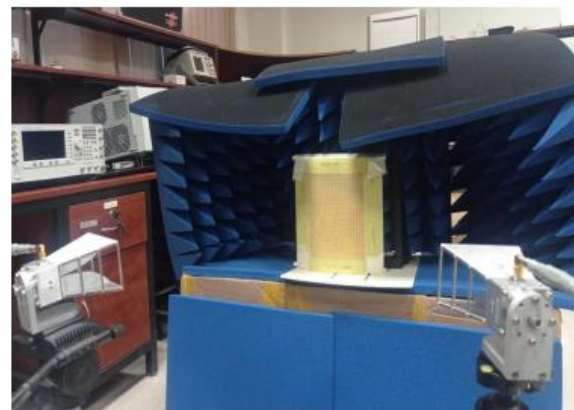
Fig.4.12 (a) Fabricated Prototype (b) Experimental Setup for conformal

Table 4: Comparison of our designed broadband MA with the recent related broadband MA designs

Ref	Broadband absorption range	Substrate thickness (mm)	Fractional bandwidth (%)	Stability at Oblique angles	Polarization insensitivity	RCS Reduction
[118]	7.8-12.6 GHz	3.2	47.0	Up-to 30˚	Yes	Not mentioned
[119]	1.91-5.75 GHz	1.6	100.26	Up-to 30˚	Not mentioned	
[120]	8-18 GHz	2.5	76.92	Up-to 30˚	Up-to φ= 90˚	
[121]	2.3-9.6 GHz	0.5	122.6	Up-to 30˚	Not mentioned	
[122]	6.7-20.58 GHz	0.8	101.7	Up-to 40˚	Up-to φ= 90˚	
[123]	15.7-23.8	1.6	41.01	Up-to 30˚	Up-to φ= 90˚	
Proposed Design	7.3-23.16 GHz	0.15	104.14	Excellent Absorption $\geq$ 90 % at θ = 45˚	Up-to φ= 90˚	Information regarding RCS reduction provided in paper for both geometries of designs i.e., (planar as well as conformal)

4.8 Discussions

The successfully fabricated and characterized novel broadband metasurface absorber, designed for applications involving RCS reduction and EM shielding, has yielded promising results. The fabricated results exhibit favorable bargain with the results extracted from CST, validating the feasibility and effectiveness of the design. The absorber showcases remarkable features, including high absorption efficiency across a wide frequency range, minimal reflectivity, and reduced radar cross-section, rendering it an exceptional candidate for diverse applications. The fabricated prototype finds practical utility in various domains, including radar stealth techniques and the mitigation of electromagnetic interference. Furthermore, experimental findings demonstrate the absorber's exceptional stability and resilience when subjected to varying angles of incidence and polarization. This study contributes significantly to the advancement of advanced electromagnetic absorber materials, offering improved performance and practical utilization possibilities.

CHAPTER 5

Electronically Re-configurable Broadband Metamaterial Absorber for Microwave Applications

Introduction

The manuscript of this chapter includes the designing and fabrication of novel electronically switchable or tunable broadband metamaterial absorber using resistors, inductors and more importantly PIN diodes. The designed metamaterial absorber consists of a square-shaped structure along with a cross circle (CC) shaped resonator. The inductors used in the outer square ring are responsible for generation of electric field within the MA unit cell while PIN diodes are used for switching ON and OFF state along with chip resistors which provide a wide characteristic broadband. The designed frequency switchable MA operates between different frequency bands i.e., during diode "**ON**" state in operates or show absorption from 8.58-9.98 GHz i.e., in C-band while in "**OFF**" state it operates between 11.65-12.67 GHz i.e., in K-band. The designed MA shows excellent absorption behavior with absorptivity rate up-to 90% for TE and TM mode for different tilted angles till 30˚ and excellent polarization insensitivity p-to φ= 90˚with absorption ≥ 90%. All the simulations of the designed MA were undertaken on CST Microwave Studio 2019 by applying flouqet port conditions.

The chapter is organized into different sections, each focusing on specific aspects. In **Section 5.1**, a geometrical approach is used to design MA. **Section 5.2** discusses the absorption phenomena related to the design of the MA. **Section 5.3** provides a detailed analysis of the absorption frequency spectra, considering variations in Phi (ϕ) and theta (θ). **Sections 5.4** and **5.5** explain the absorption physics and characteristics and distribution of the surface current density in depth. Finally, **Section 5.6** presents the concluding remarks, summarizing the main findings and insights derived from the study.

5.1 Design methodology and Simulation Analysis of the Proposed Reconfigurable MA

5.1.1 Designing Approach of the Unit Cell MA

To realize both frequency reconfigurability along with wide angular stability in metasurface design, the inclusion of symmetric structures such as circular rings or square rings is crucial. In our proposed metasurface absorber (MA), we have incorporated a square ring along with a cross-shaped circle (CC) design, ensuring excellent angular stability and polarization insensitivity. The MA absorber comprises three layers, starting with a thin copper film printed on a di-electric FR-4 substrate in the top layer, with a mere thickness of 0.3mm. A 3.25mm air spacer is introduced before attaching to the ground, which consists of a thin copper film having a conductivity of $\sigma = 5.8 \times 10^7$S/m and a 0.02mm of thickness. To achieve broadband absorption and frequency reconfigurability, we have incorporated electronic components such as resistors, inductors, and PIN diodes into the design. The geometrical configuration of our proposed MA unit cell along with 3D view is depicted in Fig. 5.1 (a-b). The top layer features conductor patterns, including a cross-circle-shaped resonator (CC), square ring structure. Furthermore, SMT resistors, diodes, and inductors are strategically integrated. The CC resonator plays a vital role in facilitating LC resonance, which generates the desired electric field. The outer square ring structure effectively directs and concentrates the electric field towards the unit cell, enabling broadband operation with the assistance of chip resistors. The PIN diodes function as switchable components, allowing for an ON/OFF state as needed. To prevent wave transmission, the bottommost layer of the MA is covered with a conductor (copper). The unit cell is meticulously designed with C-4 symmetry. The optimized parametric values are provided in **Table 5**.

Parameter	Dimensions (mm)	Parameter	Dimensions (mm)
a	8	*e*	0.22
b	2.64	*g*	0.5
c	2.97	*w*	0.5
f	3.65	*i*	0.75
h	0.32	*t*	0.02

s	3.25	m	4.22

Table 5. Augmented and optimized Parametric values of the designed MA.
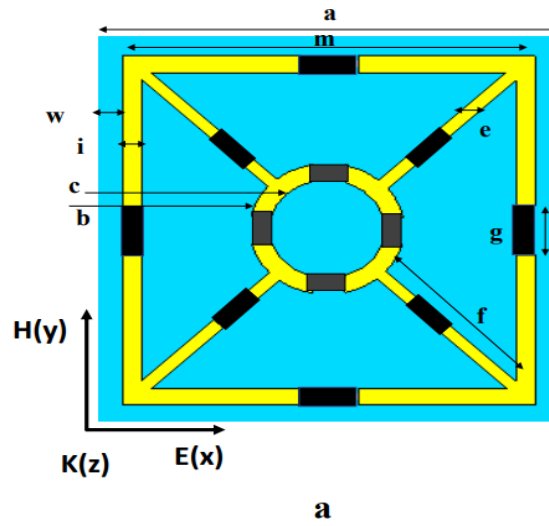
Fig.5.1 (a) Top labeled view of Unit Cell
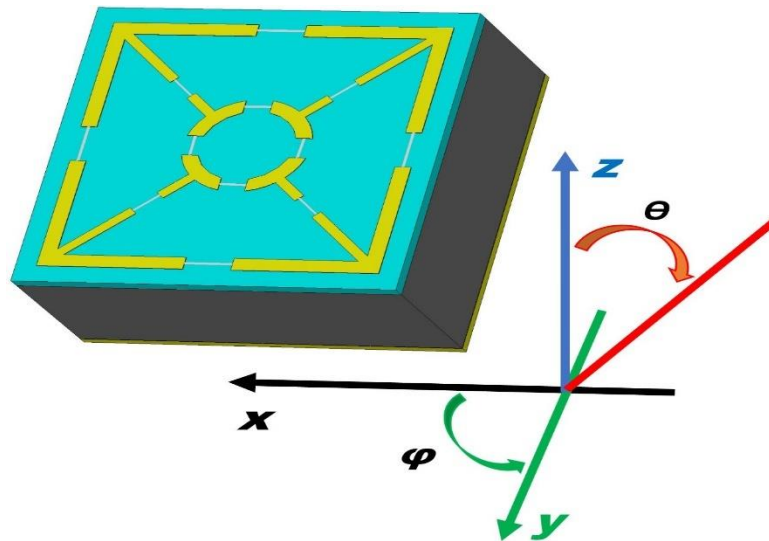
Fig.5.1 (b) 3D View of Unit Cell

5.2   Absorption Phenomena of the Suggested Meta Surface

The absorptivity factor of the metamaterial absorber when subjected to normal electromagnetic (EM) wave incidence is expressed as A(ω). This parameter quantifies the extent to which the absorber can absorb incident electromagnetic energy. Subsequently, the absorption of the proposed MA unit cell is given as:

$$A(\omega) = 1 - |S11(\omega)|^2 - |S21(\omega)|^2 \qquad (5.1)$$

In the pursuit of attaining an impeccable metamaterial absorber, the maximization of its absorption coefficient holds paramount importance. This objective can be accomplished by reducing the reflectivity (S_{11}) and transmissivity (S_{21}) coefficients. To accomplish this, careful optimization of the geometrical dimensions of the unit cell is necessary, ensuring that the absorber's impedance (Z(ω)) matches the impedance of free space (Zo), denoted as Z(ω) = Zo. By precisely adjusting the geometrical parameters of the MA, it becomes feasible to effectively suppress the reflection coefficient, driving it towards zero. This impedance-matching condition results in a substantial reduction in reflected energy, thereby augmenting the absorber's absorption performance. To further enhance the absorption coefficient, a copper metallic ground is employed. This choice of material helps to minimize the transmission coefficient ((S_{21}), driving it towards zero. Consequently, the energy that would otherwise be transmitted through the absorber is effectively blocked, contributing to a higher absorption coefficient. By accurately engineering the geometrical dimensions and leveraging the properties of copper as a ground material, the absorption coefficient A(ω) can be significantly enhanced, yielding a metamaterial absorber with improved absorption capabilities and thus has been modified to:

$$A(\omega) = 1 - |S11(\omega)|^2 \qquad (5.2)$$

Ultimately, under the incidence of normal EM wave the proposed frequency reconfigurable MA shows value of reflection coefficient i.e., S_{11} > -10 dB during diode ON state while frequency ranging from 8.5-9.9 GHz and similarly in OFF state with frequency range from

11.68-12.58 GHz show value of reflection coefficient > -10 db.

5.3   Thorough examination of the absorption frequency spectra was conducted by systematically varying the parameters Phi (ϕ) and Theta (θ).

To further validate the performance of the designed metamaterial absorber (MA) in terms of polarization insensitivity, the absorptivity was assessed by varying the polarization angle (ϕ) from 0° to 90° while maintaining consistent conditions. Through simulation conducted in CST Microwave Studio, it was observed that the proposed absorber consistently maintained its uniform performance irrespective of the polarization state, both in the ON and OFF states, as illustrated in Figure 5.2(a-b). This favorable characteristic can be attributed to the symmetrical (C-4) structure of the unit cell, which includes conducting metallic pattern, passive and active electronic components. Accordingly, the suggested absorber offers the benefit of switchable frequency bands while exhibiting robust insensitivity to variations in polarization   angles.

(a)   (b)
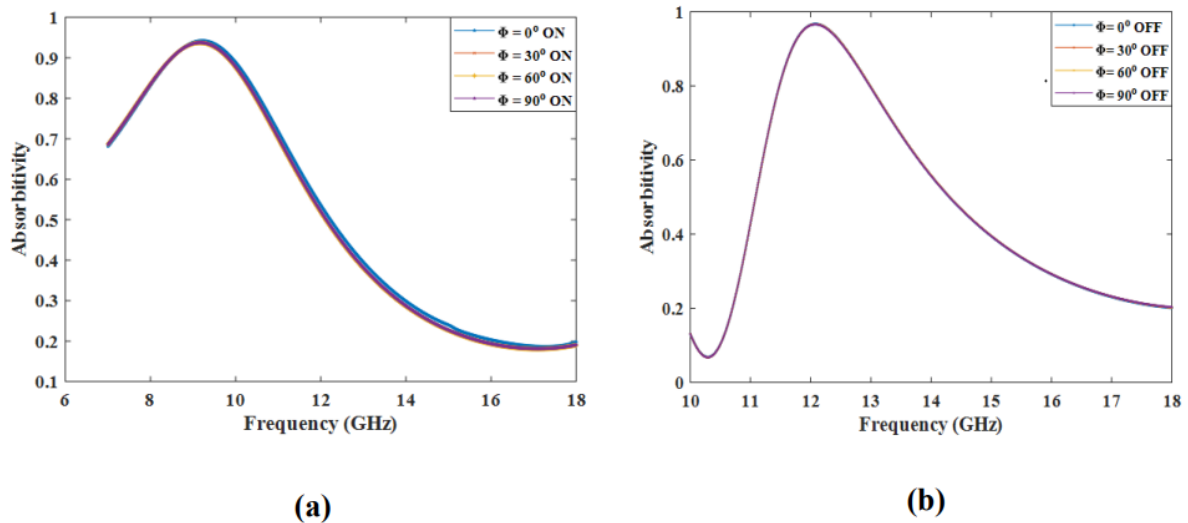
Fig. 5.2 Absorption Spectra at variation of Phi (φ)

Metamaterial absorber was thoroughly simulated and tested under various oblique incident angles. Specifically, when subjected to TE-polarized electromagnetic (EM) waves, the absorptivity was measured while varying the incidence angle from 0 to 30 degrees. Remarkably, the absorptivity consistently remained above 90% in both the ON and OFF

64

states. Similarly, when exposed to TM-polarized EM waves and by varying the angle of incidence, the absorptivity remained above 90% up to 30 degrees within the specified frequency range. This behavior was observed with the diode in both the OFF and ON states, accompanied by a marginal reduction or slight rightward shift in the absorption bands, as demonstrated in Fig. 5.3(a-d).

(a)

(b)
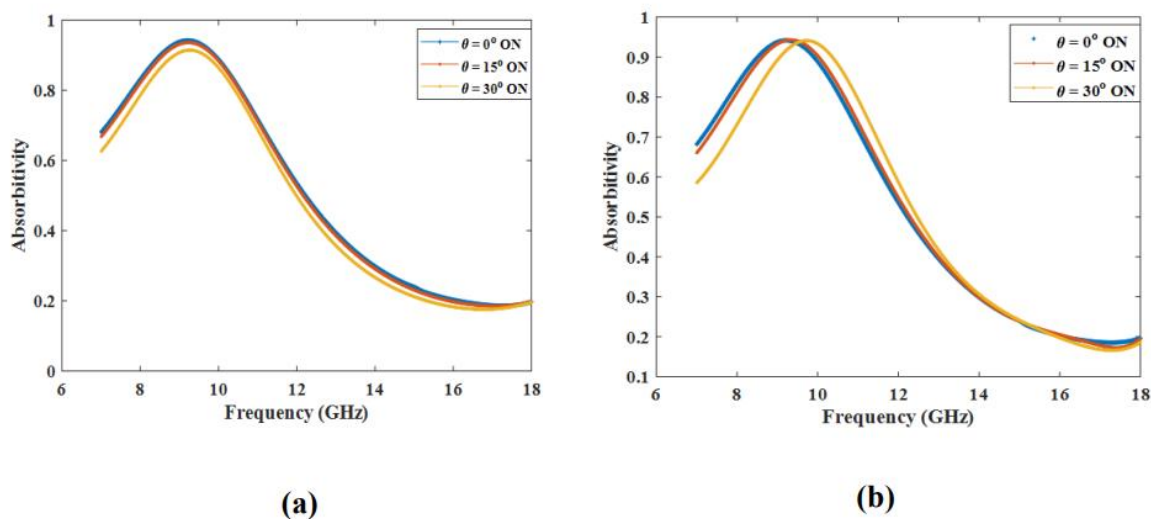
Fig. 5.3 Absorption Spectra at variation of theta (θ) in (a) TE Mode ON State (b) TM Mode ON State

(c)

(d)
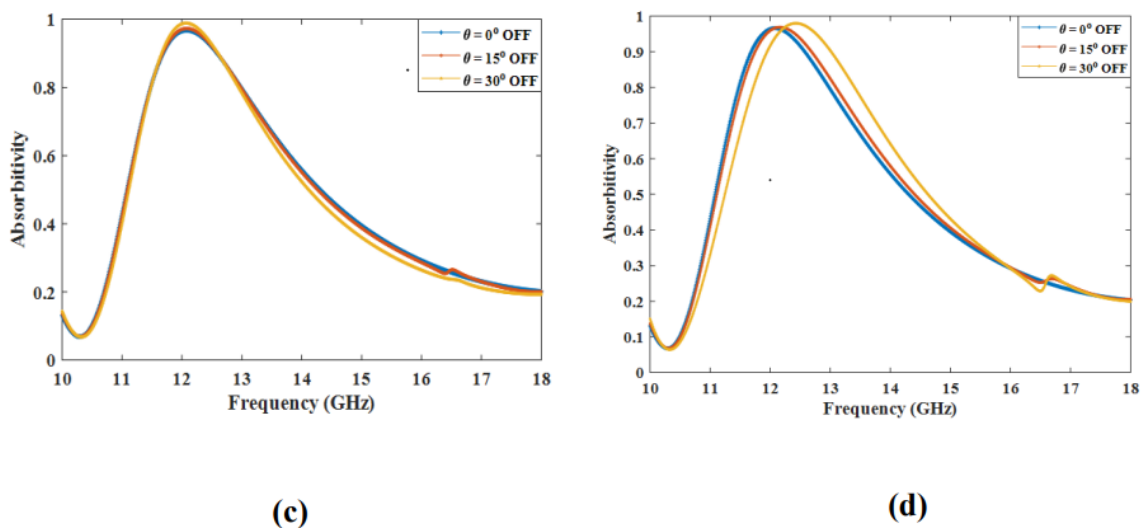
Fig. 5.3 Absorption Spectra at variation of theta (θ) in OFF State (c) TE Mode (d) TM Mode

5.4   Absorption characteristics of Proposed MA Unit Cell

To gain awareness into the absorption behavior (MA) unit cell, a detailed analysis of power loss density distribution was conducted at the operating frequencies of the designed MA, considering both the ON and OFF states. During the forward bias condition i.e., during ON state at starting frequency of 8.5 GHz in TE mode the magnitude of the power loss density was found maximum along the vertical arms of the square ring where inductors are connected, along the cross-circle shaped structure. Whereas in TM mode the power loss density has maximum concentration along the horizontal arms of square ring and completely along the cross-circle shape as shown in Fig. 5.4 (a-b). Subsequently, at highest operating frequency i.e., at 9.9 GHz in TE mode the concentration of power loss density was highest along the horizontal lengths of the square ring and minutely concentrated along the vertical lengths and for TM mode the power loss density was clustered densely around the vertical arms of the square ring and minute concentration was found along the horizontal lengths illustrated in Fig. 5.4(c-d).
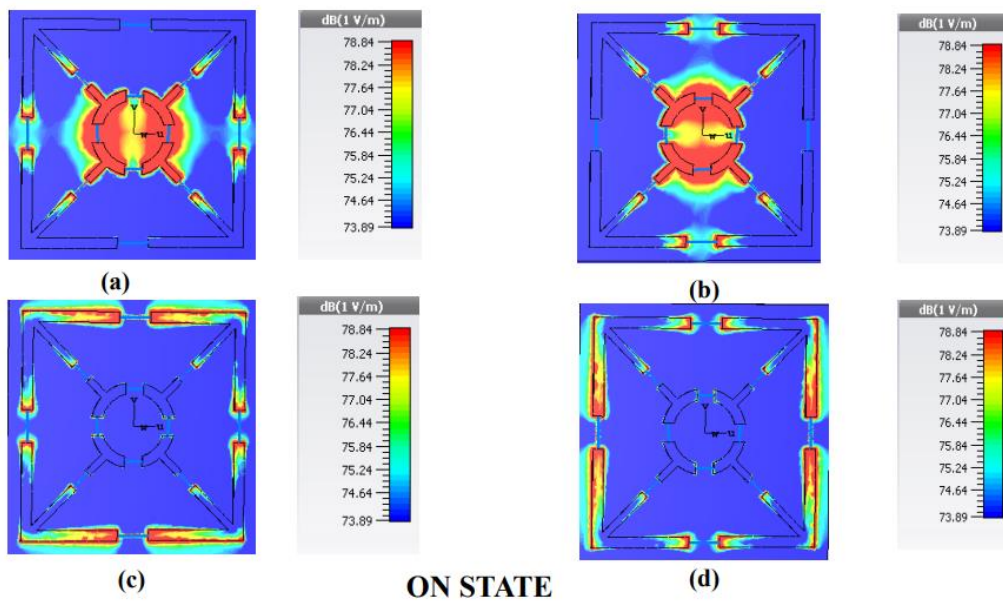
Fig.5.4 Distribution of E-Field in ON State for (a) 8.8 GHz TE Mode (b) 8.8 GHz TM Mode (c) 9.9 GHz TE Mode (d) 9.9 GHz TM Mode

Similarly, during the reverse bias condition i.e., during OFF state at 11.68 GHz in TE mode the magnitude of the power loss density was found maximum along the horizontal direction of the cross-circle shaped structure where resistors are connected and minimum along the vertical lengths of square ring where inductors are attached, similarly for TM mode the magnitude of the power loss density was found maximum along the horizontal direction of the cross-circle shaped structure where resistors are connected and minimum along the horizontal lengths of square ring where inductors are attached, as displayed in Fig. 5.5 (a-b). Correspondingly, at the highest operation frequency i.e., at 12.58 GHz in TE mode the concentration of the density of power dissipation is mostly around the horizontal lengths of the square ring and also around the cross circle-shaped structure in vertical direction and for TM mode the concentration of the density of power dissipation is generally around the vertical arms of the square ring and also around the cross circle-shaped structure in horizontal direction as depicted in Fig. 5.5 (c-d).
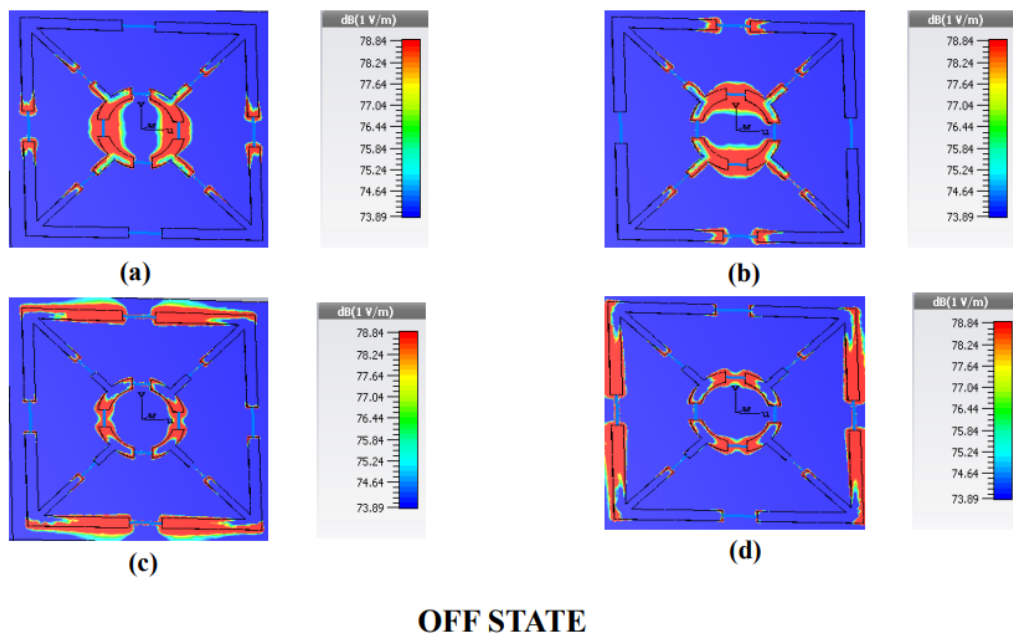
OFF STATE

Fig.5.5 Distribution of E-Field in OFF State (a) 11.680 GHz TE Mode (b) 11.680 GHz TM Mode (c) 12.581 GHz TE Mode (d) 12.581 GHz TM Mode

5.5   Distribution of Surface Current on the proposed MA Unit Cell

To gain a better understanding of the absorption mechanism, the distribution of surface current density was extensively analyzed during both forward and reverse bias conditions of the reconfigurable metamaterial absorber (MA) unit cell. In the ON state, specifically at the initial operating frequency of 8.5 GHz, the surface current exhibited an anti-parallel direction between the top metallic structure layer and the bottom ground, leading to a negative permeability. Conversely, at the final operating frequency of 9.9 GHz, the surface current flowed in a direction like that of the ground plane, resulting in negative permittivity. This behavior is illustrated in Figure 5.6(a-d). Similarly, in the OFF state (reverse bias condition), spanning the operating frequencies from 11.68 GHz to 12.58 GHz, the surface current direction was identical for both the top metallic layer and the bottom ground layer, leading to negative permittivity.
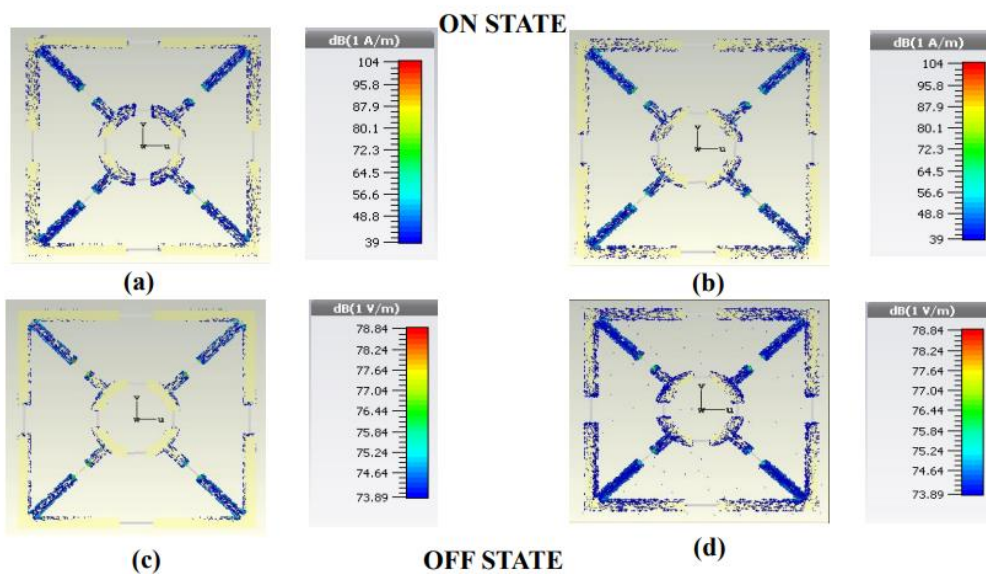
Fig.5.6 Surface Current distribution in Forward and Backward Bias conditions in (a, b), ON State (c, d) OFF State

68

Table 6: Comparison of our designed Frequency reconfigurable MA with the recent related research

	ON STATE			OFF STATE			
Research Ref	Broadband Absorption (GHz)	Fractional Bandwidth	Angular stability	Broadband Absorption	Fractional Bandwidth	Angular stability	Substrate thickness (mm)
[124]	12-12.8	0.8 (6.4%)	Not mentioned	7.1-8.1	1 (13.2%)	Not mentioned	3.175
[125]	4.75-4.85	0.1 (2%)	Not mentioned	4.0-4.15	0.1 (2%)	Not mentioned	Not mentioned
[126]	8.4-9.3	0.9 (10.2%)	Up-to 20°	9.2-10.5	1.3 (13.2%)	Up-to 20°	3.2 mm
Proposed work	8.5-9.9	1.4 (7.6%)	Up-to 30°	11.68-12.58	0.9 (3.7%)	Up-to 30°	0.3mm with excellent shifting of band from C to K-band

5.6   Conclusion:

In conclusion, this chapter represents a novel designing of electronically switchable or tunable broadband metamaterial absorbers (MAs) utilizing advanced active and passive SMT components. The proposed MA exhibits remarkable absorption characteristics across a wide frequency range, with distinct absorption bands achieved by controlling the states of the PIN diodes. Notably, the MA demonstrates excellent absorptivity rates and polarization insensitivity, maintaining high absorption levels at various oblique angles. Overall, this research offers a promising avenue for the development of efficient and adaptable metamaterial absorbers with potential applications in diverse frequency bands.

CHAPTER 6

Conclusion and Recommendations for Future

6.1   Conclusion

In conclusion, this study focused on the development and fabrication of meta material absorbers (MA) with three different designs. These designs were successfully implemented, and prototype absorbers were fabricated, providing effective performance across the C, X, K, and Ku bands. The absorbers exhibited remarkable angular stability, capable of maintaining absorption properties up to 60° of incidence angle. Additionally, they demonstrated polarization insensitivity up to 90°. One of the notable achievements of this research was the design of a frequency reconfigurable MA. This design allowed for the absorption band to be adjusted from the X band to the K-band. This flexibility in absorption frequency is of significant practical importance, as it enables the absorber to adapt to different operational requirements and frequency ranges. The successful implementation of these MA designs and their fabrication as prototypes showcased the feasibility and effectiveness of the proposed approaches. The achieved angular stability and polarization insensitivity further enhance the practical applications of the absorbers, allowing for reliable performance under various incident angles and polarization states.

Overall, this study contributes to the advancement of meta material absorbers, providing insights into MA designing and fabrication capable of covering a wide range of frequency bands while maintaining angular stability and polarization insensitivity. The frequency reconfigurable design adds an extra dimension of versatility, enabling the absorber to adapt to specific frequency requirements. These findings pave the way for the development of more efficient and adaptable absorber technologies in the future.

6.2   Future Recommendations

In conclusion, this thesis successfully achieves the goals of designing a multifunctional, multiband, broadband, and frequency-reconfigurable metasurface that demonstrates angular stability and high efficiency. However, there are opportunities for further optimization to improve both efficiency and angular stability. Here are some critical aspects to consider for future recommendations:

- Implementation of metallic patterns on flexible substrates should be explored, considering critical parameters for successful integration.
- To enhance angular stability up to 90°, a thorough parametric analysis of the geometrical configuration, periodicity, and substrate thickness is required.
- The designed metasurface serves as a perfect absorber and can be tuned to specific frequencies, enabling its applications in energy harvesting and in radar stealth.
- It is prudent to mention that substrates such as Rogers, polyimide, or gold, to amplify performance for applications that necessitate exceptional conformal stability.

These future recommendations aim to optimize the design, expand its capabilities, and explore new applications while maintaining efficiency and angular stability.

References

[1]   J. Hao, Y. Yuan, L. Ran, T. Jiang, J. A. Kong, C. Chan*, et al.*, "Manipulating electromagnetic wave polarizations by anisotropic metamaterials," *Physical review letters,* vol. 99, p. 063908, 2007.

[2]   Tang, Shiwei, Tong Cai, He-Xiu Xu, Qiong He, Shulin Sun, and Lei Zhou, "Multifunctional metasurfaces based on the "merging" concept and anisotropic single-structure meta-atoms," *Applied Sciences* 8, no. 4 (2018): 555.

[3]   Z. Li, W. Liu, H. Cheng, S. Chen, and J. Tian, "Realizing broadband and invertible linear-to-circular polarization converter with ultrathin single-layer metasurface," *Scientific reports,* vol. 5, p. 18106, 2015.

[4]   Y. Li, J. Zhang, S. Qu, J. Wang, L. Zheng, Y. Pang*, et al.*, "Achieving wide-band linear-to-circular polarization conversion using ultra-thin bi-layered metasurfaces," *Journal of Applied Physics,* vol. 117, p. 044501, 2015.

[5]   Chowdhury, Brinta, et al. "Resonant characteristics of split ring resonator and unit cell for periodic metamaterial devices." 2020 International Applied Computational Electromagnetics Society Symposium (ACES). IEEE, 2020.

[6]   Xu, Cuilian, et al. "Hybrid metasurfaces for infrared-multiband radar stealth-compatible materials applications." IEEE Access 7 (2019): 147586-147595.

[7]   H. Zhu, S. Cheung, K. L. Chung, and T. I. Yuk, "Linear-to-circular polarization conversion using metasurface," *IEEE Transactions on Antennas and Propagation,* vol. 61, pp. 4615-4623, 2013.

[8]   S. Yan and G. A. Vandenbosch, "Compact circular polarizer based on chiral twisted double split-ring resonator," *Applied Physics Letters,* vol. 102, p. 103503, 2013.

[9]   S. Hong-Yu, L. Jian-Xing, Z. An-Xue, W. Jia-Fu, and X. Zhuo, "Tri-band transparent cross-polarization converters using a chiral metasurface," *Chinese Physics B,* vol. 23, p. 118101, 2014.

[10]   Ahmed, Fahad, Tayyab Hassan, and Nosherwan Shoaib. "A multiband bianisotropic FSS with polarization-insensitive and angularly stable properties." IEEE Antennas and Wireless Propagation Letters 19.10 (2020): 1833-1837.

[11]   Y. Zheng, Y. Zhou, J. Gao, X. Cao, H. Yang, S. Li*, et al.*, "Ultra-wideband polarization conversion metasurface and its application cases for antenna radiation

enhancement and scattering suppression," *Scientific Reports,* vol. 7, p. 16137, 2017/11/23 2017.

[12]   H. Sun, C. Gu, X. Chen, Z. Li, L. Liu, B. Xu*, et al.*, "Broadband and Broad-angle Polarization-independent Metasurface for Radar Cross Section Reduction," *Scientific Reports,* vol. 7, p. 40782, 01/20/online 2017.

[13]   W. Chen, J. Gao, X. Cao, S. Li, and Z. Zhang, "A wideband multifunctional metasurface for antenna application," in *2017 Sixth Asia-Pacific Conference on Antennas and Propagation (APCAP)*, 2017, pp. 1-3.

[14]   H. F. Ma, G. Z. Wang, G. S. Kong, and T. J. Cui, "Independent Controls of Differently-Polarized Reflected Waves by Anisotropic Metasurfaces," *Scientific Reports,* vol. 5, p. 9605, 04/15/online 2015.

[15]   M.-X. Ren, W. Wu, W. Cai, B. Pi, X.-Z. Zhang, and J.-J. Xu, "Reconfigurable metasurfaces that enable light polarization control by light," *Light: Science &Amp; Applications,* vol. 6, p. e16254, 06/02/online 2017.

[16]   Rodríguez ESG, RamRakhyani AK, Schurig D, Lazzi G, Compact low-frequency metamaterial design for wireless power transfer efficiency enhancement. IEEE Transactions on Microwave Theory and Techniques. 64.5(2016) 1644-1654.

[17]   Peng XY, Wang B, Lai S, Zhang DH, Teng JH, Ultrathin multi-band planar metamaterial absorber based on standing wave resonances. Optics express. 20.25(2012) 27756-27765.

[18]   Chen HT, Antoinette JT, Nanfang Y. A review of metasurfaces: physics and applications. Reports on progress in physics 2016;79(7):076401.

[19]   Liu Y, Xiang Z, Metamaterials: a new frontier of science and technology, Chemical Society Reviews. 40.5(2011) 2494-2507.

[20]   Munk BA. Frequency selective surfaces: theory and design. Wiley-Interscience: New York; 2000.

[21]   Bilotti F, Sevgi L. Metamaterials: definitions, properties, applications, and FDTD-based modeling and simulation (Invited Paper). Int J RF Microw Comput Aided Eng 2012, 22(4):422–38.

[22]   Schurig D, Mock JJ, Justice BJ, Cummer SA, Pendry JB, Starr AF, et al. Metamaterial electromagnetic cloak at microwave frequencies. Science 2006;314(5801), 977–80.

[23]   Si LM, Lv X. CPW-FED multi-band omni-directional planar microstrip antenna using composite metamaterial resonators for wireless communications. Prog Electromagn Res 2008, 83:133–46.

[24]   Murtaza M, Rashid A, Tahir FA. A highly efficient low-cost reflective anisotropic metasurface for linear to linearly cross-and circular-polarization conversion. Microwave and Optical Technology Letters 2021;63(5):1346-1353.

[25]   Munk BA. Frequency selective surfaces. New York: John Wiley & Sons; 2000.

[26]   Wang B, Koschny T, Soukoulis CM. Wide-angle and polarization-independent chiral metamaterial absorber. Phys Rev B 2009, 80(3):0331081–83.

[27]   Veselago VG. The electrodynamics of substances with simultaneously negative values of e and l. Sov Phys Usp 1968, 10(4):509–14.

[28]   Pendry JB. Negative refraction makes a perfect lens.Phys Rev Lett 2000, 85 (18):3966–9.

[29]   Emerson WH. Electromagnetic wave absorbers and anechoic chambers through the years. IEEE Trans Antennas Propag 1973, 21(4):484–90.

[30]   Hu R, Xi W, Liu Y, Tang K, Song J, Luo X, et al. Thermal camouflaging metamaterials. Materials Today 2021;45:120-141.

[31]   Borgese M, Costa F, Genovesi S, Monorchio A, Manara G. Optimal design of miniaturized reflecting metasurfaces for ultra-wideband and angularly stable polarization conversion. Scientific reports 2018;8(1):1-11.

[32]   Gao X, Han X, Cao WP, Li HO, Ma HF, Cui TJ. Ultrawideband and high-efficiency linear polarization converter based on double V-shaped metasurface. IEEE Transactions on Antennas and Propagation 2015;63(8):3522-3530.

[33]   Mirzamohammadi F, Nourinia J, Ghobadi C, Naderali R. A dual-wideband bi-layered chiral metamaterial to develop cross-polarization conversion and asymmetric transmission functionalities for the linearly polarized electromagnetic waves. AEU-International Journal of Electronics and Communications 2019;111;152916.

[34]   Mendoza GA, Kenneth J, Arwin H. Exposing different in-depth pitches in the cuticle of the scarab beetle Cotinis mutabilis. Materials Today: Proceedings 2017;4(4):4969-4978.

[35]   Xu C, Chongxing H, Haohe H. Recent advances in structural color display of cellulose nanocrystal materials. Applied Materials Today 2021;22:100912.

[36] Qi Y, Yang S, Wang J, Li L, Bai Z, Wang, Y, et al. Recent advance of emerging low-dimensional materials for vector soliton generation in fiber lasers. Materials Today Physics 2022;100622.

[37] Zeng Q, Ren W, Zhao H, Xue Z, Li W. Dual-band transmission-type circular polariser based on frequency selective surfaces. IET Microwaves, Antennas \& Propagation 2019;13(2):216-222.

[38] Zhu J, Yang Y, McGloin D, Unnithan RR, Li S, Liao S, et al. 3-D printed planar dielectric linear-to-circular polarization conversion and beam-shaping lenses using coding polarizer. IEEE Transactions on Antennas and Propagation 2020;68(6):4332-4343.

[39] Carranza IE, Grant JP, Gough J, Cumming D. Terahertz metamaterial absorbers implemented in CMOS technology for imaging applications: scaling to large format focal plane arrays. IEEE Journal of Selected Topics in Quantum Electronics 2016;23(4):1-8.

[40] Lim, Daecheon, Dongju L, Sungjoon L. Angle-and polarization-insensitive metamaterial absorber using via array. Scientific reports 2016;6(1):1-9.

[41] Luo Z, Ji S, Zhao J, Wu H, Dai H. A multiband metamaterial absorber for GHz and THz simultaneously. Results in Physics 2021;30:104893.

[42] Wang BX, He Y, Lou P, Huang WQ, Pi F. Penta-band terahertz light absorber using five localized resonance responses of three patterned resonators. Results in Physics 2020;16:102930.

[43] Cheng Y, Zou Y, Luo H, Chen F, Mao X. Compact ultra-thin seven-band microwave metamaterial absorber based on a single resonator structure. Journal of Electronic Materials 2019;48(6):3939-3946.

[44] Cheng, Yongzhi, Hui L, Fu C. Broadband metamaterial microwave absorber based on asymmetric sectional resonator structures. Journal of Applied Physics 2020;127(21):214902.

[45] Pan W, Shen T, Ma Y, Zhang Z, Yang H, Wang X, et al. Dual-band and polarization-independent metamaterial terahertz narrowband absorber. Applied Optics 2021;60(8):2235-2241.

[46] Kalraiya, Sachin, Kumar R, Chaudhary, Gangwar RK. Polarization independent triple band ultrathin conformal metamaterial absorber for C-and X-frequency bands. AEU-

International Journal of Electronics and Communications 2021;135:153752.

[47]   Singh, Kumar R, Gupta A. A wrenched-square shaped polarization independent and wide angle stable ultra-thin metamaterial absorber for s-band, x-band and ku-band applications. AEU-International Journal of Electronics and Communications 2021;132:153648.

[48]   Karaaslan M, Bağmancı M, Ünal E, Akgol O, Altıntaş O, Sabah C. Broad band metamaterial absorber based on wheel resonators with lumped elements for microwave energy harvesting. Optical and Quantum Electronics 2018;50(5):1-18.

[49]   Pendry JB, Holden AJ, Robbins DJ, Stewart WJ. Magnetism from conductors and enhanced nonlinear phenomena. IEEE Trans Microw Theory Technol 1999, 47 (11):2075–84.

[50]   Chetan Barde, Arvind Choubey, and Rashmi Sinha. Wide band metamaterial absorber for Ku and K band applications J. Appl. Phys. 126, 175104 (2019).

[51]   Landy NI, Sajuyigbe S, Mock JJ, Smith DR, Padilla WJ. Perfect metamaterial absorber. Phys Rev Lett 2008, 100(20):2074021–24.

[52]   Yadgar I. Abdulkarim, Lianwen Deng, Olcay Altıntaş, Emin Ünal, Muharrem Karaaslan. Metamaterial absorber sensor design by incorporating swastika shaped resonator to determination of the liquid chemicals depending on electrical characteristics Physica E: Low-dimensional Systems and Nanostructures (114) 2019.

[53]   Yongzhi cheng, Yao zou, Hui luo, Fu chen, and Xuesong mao. Compact Ultra-Thin Seven-Band Microwave Metamaterial Absorber Based on a Single Resonator Structure, Journal of ELECTRONIC MATERIALS https://doi.org/10.1007/s11664-019-07156-z.

[54]   Saif Hannan, Mohammad Tariqul Islam, Ahasanul Hoque, Mandeep Jit Singh and Ali F. Almutairi, Design of a Novel Double Negative Metamaterial Absorber Atom for Ku and K Band Applications, Electronics 2019.

[55]   Fereshteh Sadat Jafari, Mohammad Naderi, Ahmad Hatami, Ferdows B. Zarrabi, Microwave Jerusalem cross absorber by metamaterial split ring resonator load to obtain polarization independence with triple band application, Int. J. Electron. Commun. (AEÜ) 101 (2019) 138–144.

[56]   Wei Bing Lu, Jian Wei Wang, Jin Zhang, Zhen Guo Liu, Hao Chen, Wei Jie Song, Zhi Hao Jiang, Flexible and optically transparent microwave absorber with wide

bandwidth based on graphene, Carbon 152 (2019) 70e76.

[57]   Kavitha Muthukrishnan & Venkateswaran Narasimhan, An Ultra-Thin Triple-Band Polarization Independent Wide-Angle Microwave Metamaterial Absorber, Plasmonics https://doi.org/10.1007/s11468-019-00985-y.

[58]   Prakash Ranjan, Arvind Choubey, Santosh Kumar Mahto, Rashmi Sinha & Chetan Barde, A novel ultrathin wideband metamaterial absorber for X-band applications 2019 https://www.tandfonline.com/loi/tewa20.

[59]   Ning, Jing, et al. "Ultra-broadband microwave absorption by ultra-thin metamaterial with stepped structure induced multi-resonances." Results in Physics 18 (2020): 103320.

[60]   Guang sheng Deng et al, "An Ultrathin, Triple-Band Metamaterial Absorber with Wide-Incident-Angle Stability for Conformal Applications at X and Ku Frequency Band", Nanoscale research letters, 2020.

[61]   Saif Hannan et al, "Angle-insensitive co-polarized metamaterial absorber based on equivalent circuit analysis for dual band WiFi applications", Scientific Reports-11, Article Number:13791, 2021.

[62]   Jie Qian et al, "Hybrid perfect metamaterial absorber for microwave spin rectification applications", Scientific Reports-10, Article Number:19240, 2020.

[63]   Javad Shabanpour et al, "Reconfigurable honeycomb metamaterial absorber having incident angular stability", Scientific Reports-10, Article Number:14920, 2020.

[64]   Saif Hannan et al, "Wide Bandwidth Angle- and Polarization-Insensitive Symmetric Metamaterial Absorber for X and Ku Band Applications", Scientific Reports-10, Article Number:10338, 2020.

[65]   Yan-Lin Liao and Yan Zhao, "Ultra-narrowband dielectric metamaterial absorber with ultra sparse nanowire grids for sensing applications", Scientific Reports-10 Article Number:1480, 2020.

[66]   Ahmed Elsharabasy et al, "Wide-angle, wide-band, polarization-insensitive metamaterial absorber for thermal energy harvesting", Scientific Reports-10 Article Number:16215, 2020.

[67]   Mehmet Ba gmancı, O guzhan Akgöl, Meliks ¸ah Özaktürk, Muharrem Karaaslan, Emin Ünal, Mehmet Bakır, Polarization independent broadband metamaterial absorber for microwave applications2019, https://doi.org/10.1002/mmce.21630.

77

[68]   Kavitha Muthukrishnan1 & Venkateswaran Narasimhan, An Ultra-Thin Triple-Band Polarization-Independent Wide-Angle Microwave Metamaterial Absorber, Plasmonics 2019, https://doi.org/10.1007/s11468-019-00985-y

[69]   Xiaoqi Shao, Jiahui Fu, Bo Lv, Wan Chen, Ultrathin broadband absorber based on metamaterials 2019.

[70]   Jiakun Song, Cheng Huang, Jianing Yang, Xu Zhang, Jinqiang Peng, and Xiangang Luo, Broadband and Tunable Radar Absorber Based on Graphene Capacitor Integrated with Resistive Frequency Selective Surface, DOI 10.1109/TAP.2019.2943419, IEEE Transactions on Antennas and Propagation 2019.

[71]   Mohammad Lutuf Hakim et al, "Polarization insensitivity characterization of dual-band perfect metamaterial absorber for K band sensing applications", Scientific Reports, Vol-11, P:1-14, 2021.

[72]   Xiaoming Liu et al, "Dual-band metamaterial perfect absorber based on artificial dielectric "molecules", Scientific Reports, Article Number.6, 2016.

[73]   Yunsong Xie et al, "A subwavelength resolution microwave/6.3 GHz camera based on a metamaterial absorber", Scientific Reports-7, Article Number:40490, 2017.

[74]   Lincy Stephen et al, "Realization of Bidirectional, Bandwidth-Enhanced Metamaterial Absorber for Microwave Applications", Scientific Reports-9 Article Number:10058, 2019.

[75]   Majid Amiri et al, "Soil moisture remote sensing using SIW cavity based metamaterial perfect absorber", Scientific Reports-11 Article Number:7153, 2021.

[76]   Nassim Chikhi et al, "Pyramidal metamaterial absorber for mode damping in microwave resonant structures", Scientific Reports-10 Article Number:19352, 2020.

[77]   Keng-Te Lin et al, "Structured graphene metamaterial selective absorbers for high efficiency and omnidirectional solar thermal energy conversion", Scientific Reports-10 Article Number:1389, 2020.

[78]   R.M.H. Bilal et al, "Elliptical metallic rings-shaped fractal metamaterial absorber in the visible regime", Scientific Reports-10 Article Number:14035, 2020.

[79]   Cuong Manh Tran1 & Hai Van Pham1 & Hien Thuy Nguyen1 & Thuy Thi Nguyen1 & Lam Dinh Vu2 & Tung Hoang Do, Creating Multiband and Broadband Metamaterial Absorber by Multiporous Square Layer Structure 2019, https://doi.org/10.1007/s11468-019-00953-6.

[80] Peng Zhou 1, Qiulin Huang 1*, Lei Ji 2, and Xiaowei Shi, Design of a Thin Broadband Metamaterial Absorber Based on Resistance Frequency Selective Surface, ACES JOURNAL, Vol. 34, No. 10, October 2019.

[81] Xinru Lu 1, Juan Chen 2, Youqi Huang 3, Zixian Wu 1, and Anxue Zhang, Design of Ultra-wideband and Transparent Absorber based on Resistive Films, ACES JOURNAL, Vol. 34, No. 5, May 2019.

[82] Guo Wen ZHANG, Jun GAO, Xiangyu CAO, HuanHuan YANG, Liaori JIDI, An Ultra-Thin Low-Frequency Tunable Metamaterial Absorber Based on Lumped Element, RADIOENGINEERING, VOL. 28, NO. 3, SEPTEMBER 2019.

[83] Ke Chen, Xinyao Luo, Guowen Ding, Junming Zhao, Yijun Feng, and Tian Jiang, Broadband microwave metamaterial absorber with lumped resistor loading 2019, https://doi.org/10.1051/epjam/2018011.

[84] Sachin Kalraiya, Raghvendra Kumar Chaudhary, and Mahmoud A. Abdalla, Design and analysis of polarization independent conformal wideband metamaterial absorber using resistor loaded sector shaped resonators, J. Appl. Phys. 125, 134904 (2019); doi: 10.1063/1.5085253

[85] Debidas Kundu, Sharad Baghel, Akhilesh Mohan, and Ajay Chakrabarty, Design and Analysis of Printed Lossy Capacitive Surface Based UltraWideband Low-Profile Absorber, DOI 10.1109/TAP.2019.2902660, IEEE Transactions on Antennas and Propagation 2019.

[86] Saurabh Sambhav, X-Band metamaterial wide-band polarization insensitive thin absorber using Lumped Resistor, URSI AP-RASC 2019.

[87] Jianfeng Wei, Yun He, Shaowei Bie, Song Wu, Zhipeng Lei, Wei Deng, Yutong Liu, Yulu Zhang, Chengli Li, Junqiang Ai and Jianjun Jiang, Flexible design and realization of wideband microwave absorber with double-layered resistor loaded FSS, J. Phys. D: Appl. Phys. 52 (2019) 185101 (8pp).

[88] Qi Yuan1, Hua Ma1, Sai Sui1, Yang Shen1, Jiafu Wang1, Mingde Feng1, Hongya Chen1, Yao Jing1, Xiaofeng Wang1 Shaobo Qu, A Broadband Wide-angle Synthetical Absorber Designed by Topology Optimization of Resistance Surface and Metal Wires, DOI 10.1109/ACCESS.2019.2942495, IEEE Access.

[89] Cuilian Xu, "Hybrid metasurfaces for infrared-multiband radar stealth-compatible materials applications", IEEE Access, 2020.

[90] Heijun Jeong et al, "Subwavelength Metamaterial Unit Cell for Low-Frequency Electromagnetic Absorber Applications", Scientific Reports-8, Article Number:16774, 2018.

[91] H. Zhao, X. Wang, J. He, J. Guo, J. Ye, Q. Kan, *et al.*, "High-efficiency terahertz devices based on cross-polarization converter," *Scientific Reports,* vol. 7, p. 17882, 2017/12/20 2017.

[92] D. Wang, Y. Gu, Y. Gong, C.-W. Qiu, and M. Hong, "An ultrathin terahertz quarter-wave plate using planar babinet-inverted metasurface," *Optics Express,* vol. 23, pp. 11114-11122, 2015/05/04 2015.

[93] Q. Hong, T. X. Wu, X. Zhu, R. Lu, and S.-T. Wu, "Designs of wide-view and broadband circular polarizers," *Optics Express,* vol. 13, pp. 8318-8331, 2005/10/03 2005.

[94] Engineering Simulation & 3D Design Software | CST Microwave Studio. Available online: https://www.3ds.com (accessed on 7 April 2019).

[95] Peng XY, Wang B, Lai S, Zhang DH, Teng JH. Ultrathin multi-band planar metamaterial absorber based on standing wave resonances. Optics express 2012;20(25):27756-27765.

[96] Shang S, Yang S, Tao L, Yang L, Cao H. Ultrathin triple-band polarization-insensitive wide-angle compact metamaterial absorber. AIP Advances 2016;6(7):075203.

[97] Hoque A, Islam MT, Almutairi AF, et al. SNG and DNG meta-absorber with fractional absorption band for sensing application. Scientific reports 2020;10(1):1-17.

[98] Amiri M, Tofigh F, Shariati M, et al. Review on metamaterial perfect absorbers and their applications to IoT. IEEE Internet of Things Journal 2020;8(6): 4105-4131.

[99] Dawood A. Finite difference time-domain modelling of metamaterials: Gpu implementation of cylindrical cloak. Advanced Electromagnetics 2013;2(2):10-17.

[100] Ghosh S, Srivastava KV. An equivalent circuit model of FSS-based metamaterial absorber using coupled line theory. IEEE Antennas and Wireless Propagation Letters 2014;14:511-514.

[101] Li SJ, Wu PX, Xu HX, et al. Ultra-wideband and polarization-insensitive perfect absorber using multilayer metamaterials, lumped resistors, and strong coupling effects. Nanoscale research letters 2018;13(1):1-13.

[102] Xu HX, Wang GM, Qi MQ, Liang JG,et al. Triple-band polarization-insensitive wide-angle ultra-miniature metamaterial transmission line absorber. Physical Review B 2012;86(20):205104.

[103] Shapiro MA, Shvets G, Sirigiri JR, Temkin RJ. Spatial dispersion in metamaterials with negative dielectric permittivity and its effect on surface waves. Optics letters 2006;31(13):2051-2053.

[104] Garg P, Jain P. Novel ultrathin penta-band metamaterial absorber. AEU-International Journal of Electronics and Communications 2020;116:153063.

[105] Sekar RAMYA, Inabathini SR. An ultra-thin compact wideband metamaterial absorber. Radioengineering 2018;27(2):365.

[106] Li SJ, Wu PX, Xu HX, Zhou YL, Cao XY, Han JF, et al. Ultra-wideband and polarization-insensitive perfect absorber using multilayer metamaterials, lumped resistors, and strong coupling effects. Nanoscale research letters 2018;13(1):1-13.

[107] Bhattacharyya, Somak, Ghosh S, Srivastva KV. A microwave metamaterial absorber with wide bandwidth. URSI Asia-Pacific Radio Science Conference (URSI AP-RASC). IEEE, 2016.

[108] Mol, Libi VA, Aanandan CK. An ultrathin microwave metamaterial absorber with enhanced bandwidth and angular stability. Journal of physics Communications 2017;1(1):015003.

[109] Ding F, Cui Y, Ge X, Jin Y, He S. Ultra-broadband microwave metamaterial absorber. Applied physics letters 2012;100(10):103506.

[110] Mishra, Kumar R, Gupta RD, Datar S. Metamaterial Microwave Absorber (MMA) for Electromagnetic Interference (EMI) Shielding in X-Band. Plasmonics 2021;16(6):2061-2071.

[111] Sood, Deepak, Tripathi CC. A compact ultrathin ultra-wideband metamaterial microwave absorber. Journal of Microwaves, Optoelectronics and Electromagnetic Applications 2017;16:514-528.

[112] Nguyen, TT, Lim S. Angle-and polarization-insensitive broadband metamaterial absorber using resistive fan-shaped resonators. Applied Physics Letters 2018;112(2):021605.

[113] Deng G, Lv K, Sun H, Hong Y, Zhang X, Yin Z, et al. An ultra-wideband, polarization insensitive metamaterial absorber based on multiple resistive film layers

with wide-incident-angle stability. IJMWT 2021;13(1):58-66.

[114] Li S, Gao J, Cao X, Zhang Z, Zheng Y, Zhang C. Multiband and broadband polarization-insensitive perfect absorber devices based on a tunable and thin double split-ring metamaterial. Optics Express 2015;23(3):3523-3533.

[115] Chen T, Li SJ, Cao XY, Gao J, Guo ZX. Ultra-wideband and polarization-insensitive fractal perfect metamaterial absorber based on a three-dimensional fractal tree microstructure with multi-modes. Applied Physics A 2019;125(4):1-8.

[116] Xiong H, Hong J, Luo C, Zhong L. An ultrathin and broadband metamaterial absorber using multi-layer structures. Journal of Applied Physics 2013;114:064109.

[117] Liu, Tian, Kim SS. Ultrawide bandwidth electromagnetic wave absorbers using a high-capacitive folded spiral frequency selective surface in a multilayer structure. Scientific reports 2019;9(1):1-10.

[118] T. Q.H. Nugyen, T.K.T. Nugyen, T. N. Cao, H. Nugyen., L.G.,Bach, "Numerical study of a broadband metamaterial absorber using a single split circle ring and lumped resistors for X-band   applications." AIP Advances, Vol10, PP-035326, 2020.

[119] N. Hakla, S. Ghosh, and K. V. Srivastava, "Design of low profile broadband capacitive circuit absorber, IET Electronics Lett., vol 52, no. 22, 2016.

[120] Nguyen, T. K. T. et al. Simple design of a wideband and wide-angle insensitive metamaterial absorber using lumped resistors for X-and Ku-bands. IEEE Photonics J. (2021).

[121] J, Cao X, Gao J, Cong L, Wang S and Yang H (2018) Design of miniaturized wideband microwave absorber loaded with lumped resistance. Radio engineering 27, 747

[122] S. Sambhav, J. Ghosh, A. K. Singh, "Ultra-Wideband Polarization Insensitive Thin Absorber Based on Resistive Concentric Circular Rings IEEE Transactions on Electromagnetic combability, Vol 10, PP-1109, 2021.

[123] R Y. Khanna, Y.K. Awashti. "Wideband Ultra-thin Metamaterial Absorber for Ku & K-Band Applications. "Scientific Reports, Vol 12, PP-14992, 2020.

[124] Turpin, J. P., Bossard, Ja, Morgan, K. L., Werner, D. H. & Werner, P. L. Reconfigurable and Tunable Metamaterials: A Review of the Theory and Applications. Int. J. Antennas Propag 2014, 1–18, doi:10.1155/2014/429837 (2014).

[125] Xu, W. & Sonkusale, S. Microwave diode switchable metamaterial reflector / absorber Microwave diode switchable metamaterial reflector/absorber. Appl. Phys. Lett. 031902, 3–7, doi:10.1063/1.4813750 (2014).

[126] Li S. J., Lee, D., Jeong, H. & Lim, S. Electronically Switchable Broadband Metamaterial Absorber. Scientifc Reports. 7, 4891 (2017).

[127] Thummaluru SR, Mishra N, Chaudhary RK, Design and analysis of an ultrathin triple-band polarization independent metamaterial absorber. AEU-International Journal of Electronics and Communications. 82(2017) 508-515.

[128] Moniruzzaman M, Islam MT, Muhammad G, Singh MSJ, Samsuzzaman M, Quad band metamaterial absorber based on asymmetric circular split ring resonator for multiband microwave applications. Results in Physics. 19(2020) 103467.

[129] Singh AK, Abegaonkar MP, Koul SK, Dual-and triple-band polarization insensitive ultrathin conformal metamaterial absorbers with wide angular stability. IEEE Transactions on Electromagnetic Compatibility. 61.3(2018) 878-886.

[130] Wang, Qi, Yongzhi C. Compact and low-frequency broadband microwave metamaterial absorber based on meander wire structure loaded resistors. AEU-international Journal of Electronics and Communications 2020;120:153198.

[131] Yu P, Besteiro LV, Huang Y, Wu J, Fu L, Tan HH, et al. Broadband metamaterial absorbers. Advanced Optical Materials 2019;7(3):1800995.

[132] P. Tiwari, S. K. Pathak, and V. Siju. "Design, development and characterization of resistive arm based planar and conformal. metasurfaces for RCS reduction," Scientific Reports (2022).